J|A|C|S ARTICLES

Published on Web 07/08/2009

Protein Hydration Dynamics and Molecular Mechanism of Coupled Water−Protein Fluctuations

Luyuan Zhang, Yi Yang, Ya-Ting Kao, Lijuan Wang, and Dongping Zhong*

Departments of Physics, Chemistry, and Biochemistry, Programs of Biophysics, Chemical Physics, and Biochemistry, 191 West Woodruff Avenue, The Ohio State University, Columbus, Ohio 43210

Received May 8, 2009; E-mail: dongping@mps.ohio-state.edu

Abstract: Protein surface hydration is fundamental to its structural stability and flexibility, and water−protein fluctuations are essential to biological function. Here, we report a systematic global mapping of water motions in the hydration layer around a model protein of apomyoglobin in both native and molten globule states. With site-directed mutagenesis, we use intrinsic tryptophan as a local optical probe to scan the protein surface one at a time with single-site specificity. With femtosecond resolution, we examined 16 mutants in two states and observed two types of water-network relaxation with distinct energy and time distributions. The first water motion results from the local collective hydrogen-bond network relaxation and occurs in a few picoseconds. The initial hindered motions, observed in bulk water in femtoseconds, are highly suppressed and drastically slow down due to structured water-network collectivity in the layer. The second water-network relaxation unambiguously results from the lateral cooperative rearrangements in the inner hydration shell and occurs in tens to hundreds of picoseconds. Significantly, this longtime dynamics is the coupled interfacial water−protein motions and is the direct measurement of such cooperative fluctuations. These local protein motions, although highly constrained, are necessary to assist the longtime water-network relaxation. A series of correlations of hydrating water dynamics and coupled fluctuations with local protein's chemical and structural properties were observed. These results are significant and reveal various water behaviors in the hydration layer with wide heterogeneity. We defined a solvation speed and an angular speed to quantify the water-network rigidity and local protein flexibility, respectively. We also observed that the dynamic hydration layer extends to more than 10 Å. Finally, from native to molten globule states, the hydration water networks loosen up, and the protein locally becomes more flexible with larger global plasticity and partial unfolding.

Introduction

Protein surface hydration is essential to its structural stability and flexibility and protein−associate water often is an integral element in biological activities.[1−13] Water−protein interactions are fundamental to protein structural and functional behaviors such as in governing protein glass transition,[14−18] facilitating protein folding,[19−23] maintaining structural integrity,[24−27] mediating molecular recognition,[3,4,28−32] and accelerating enzy-

(1) Ball, P. *Chem. Rev.* **2008**, *108*, 74–108. Ball, P. *ChemPhysChem* **2008**, *9*, 2677–2685.
(2) Chaplin, M. *Nat. Rev. Mol. Cell Biol.* **2006**, *7*, 861–866.
(3) Pal, S. K.; Zewail, A. H. *Chem. Rev.* **2004**, *104*, 2099–2123. Pal, S. K.; Peon, J.; Bagchi, B.; Zewail, A. H. *J. Phys. Chem. B* **2002**, *106*, 12376–12395.
(4) Levy, Y.; Onuchic, J. N. *Annu. Rev. Biophys. Biomol. Struct.* **2006**, *35*, 389–415.
(5) Rasaiah, J. C.; Garde, S.; Hummer, G. *Annu. Rev. Phys. Chem.* **2008**, *59*, 713–740.
(6) Bagchi, B. *Chem. Rev.* **2005**, *105*, 3197–3219.
(7) Wuthrich, K. *Angew. Chem., Int. Ed.* **2003**, *42*, 3340–3363.
(8) Mattos, C. *Trends Biochem. Sci.* **2002**, *27*, 203–208.
(9) Makarov, V.; Pettitt, B. M.; Feig, M. *Acc. Chem. Res.* **2002**, *35*, 376–384.
(10) McCoustra, M. R. S. *Faraday Discuss.* **2009**, *141*, 1–488, and references therein.
(11) Daniel, R. M.; Finney, J. L.; Stoneham, M. *Philos. Trans. R. Soc. London, Ser. B* **2004**, *359*, 1143–1328, and references therein.
(12) Frauenfelder, H.; Chen, G.; Berendzen, J.; Fenimore, P. W.; Jansson, H.; McMahon, B. H.; Stroe, I. R.; Swenson, J.; Young, R. D. *Proc. Natl. Acad. Sci. U.S.A.* **2009**, *106*, 5129–5134. Fenimore, P. W.; Frauenfelder, H.; McMahon, B. H.; Parak, F. G. *Proc. Natl. Acad. Sci. U.S.A.* **2002**, *99*, 16047–16051. Frauenfelder, H.; Fenimore, P. W.; Chen, G.; McMahon, B. H. *Proc. Natl. Acad. Sci. U.S.A.* **2006**, *103*, 15469–15472. Fenimore, P. W.; Frauenfelder, H.; McMahon, B. H.; Young, R. D. *Proc. Natl. Acad. Sci. U.S.A.* **2004**, *101*, 14408–14413.
(13) Zhong, D. *Adv. Chem. Phys.* **2009**, *143*, 83–149.
(14) Vitkup, D.; Ringe, D.; Petsko, G. A.; Karplus, M. *Nat. Struct. Biol.* **2000**, *7*, 34–38.
(15) Tarek, M.; Tobias, D. J. *Phys. Rev. Lett.* **2002**, *88*, 138101.
(16) Tournier, A. L.; Xu, J.; Smith, J. C. *Biophys. J.* **2003**, *85*, 1871–1875.
(17) Chen, S.-H.; Liu, L.; Fratini, E.; Baglioni, P.; Faraone, A.; Mamontov, E. *Proc. Natl. Acad. Sci. U.S.A.* **2006**, *103*, 9012–9016.
(18) Pradeep, K.; Yan, Z.; Xu, L.; Mazza, M. G.; Buldyrev, S. V.; Chen, S.-H.; Sastry, S.; Stanley, H. E. *Phys. Rev. Lett.* **2006**, *97*, 177802.
(19) Cheung, M. S.; Garcia, A. E.; Onuchic, J. N. *Proc. Natl. Acad. Sci. U.S.A.* **2002**, *99*, 685–690. Shea, J.-E.; Onuchic, J. N.; Brooks, C. L. *Proc. Natl. Acad. Sci. U.S.A.* **2002**, *99*, 16064–16068.
(20) Kim, S. J.; Born, B.; Havenith, M.; Gruebele, M. *Angew. Chem., Int. Ed.* **2008**, *47*, 6486–6489.
(21) Kimura, T.; Maeda, A.; Nishiguchi, S.; Ishimori, K.; Morishima, I.; Konno, T.; Goto, Y.; Takahashi, S. *Proc. Natl. Acad. Sci. U.S.A.* **2008**, *105*, 13391–13396.
(22) Daidone, I.; Ulmschneider, M. B.; Di Nola, A.; Amadei, A.; Smith, J. C. *Proc. Natl. Acad. Sci. U.S.A.* **2007**, *104*, 15230–15235.

matic catalysis.[33−37] Thus, characterization of dynamic behaviors of biological water is critical to understanding its role in these biological processes. Various methods and strategies[38−44] have been used to tackle this longstanding unsolved problem in protein science. We have recently developed a methodology,[13,45−48] combining femtosecond spectroscopy and site-directed mutagenesis, to study protein hydration dynamics and water−protein coupling fluctuations using intrinsic tryptophan (Trp) as a local optical probe. We were able to place the probe to any desirable position through site-directed mutations, and we have examined a series of proteins in different structures and states ranging from random coil, to α-helix and to self-assembly of oligomers,[49] from recognition state to various pH-induced isomers in drug delivery through conformation transitions,[50] and from charge-rich native to hydrophobic mutant configurations in examining protein-residue solvation[51] and active-site solvation.[52] For all systems studied, we observed a robust, distinct biphasic distribution of relaxation in a few and tens to hundreds of picoseconds. The former is attributed to initial local collective water-network relaxation, and the latter is assigned to water-network lateral restructuring, facilitated by local protein fluctuations. These results showed that water relaxations are dominant and protein contributions could be minor. However, a series of important issues still need to be addressed, for example, global heterogeneity of the hydration dynamics around protein surfaces, correlations between the dynamics with protein local structures and chemical identities, and molecular mechanisms of coupled water−protein fluctuations.

We report here our direct global surface mapping of hydration dynamics and water−protein interactions around a globular α-helical protein, apomyoglobin (apoMb), in its two states, native (N) and molten globule (MG), using intrinsic tryptophan residue as a local molecular probe to scan the surface by protein engineering. A brief summary of this extensive study has appeared earlier,[53] and here we give a full account of the global mapping of these water dynamics with detailed description of observed various correlations and their relationship to protein's structure and dynamics. Figure 1 shows the possible structures of apoMb in two states, based on the X-ray crystal structure (PDB ID: 1MBD) of sperm whale myoglobin in its holo-form[54] and the extensive NMR studies,[55−57] with the designed mutation sites in yellow balls. Myoglobin, the main oxygen transporter in muscle, has ∼75% helical content with eight helices, namely A−H. In apo-form, on removal of the prosthetic heme group, the F helix and the N-terminus of the G helix become random coils, and the rest of the protein remains an intact globular helical structure. The protein can be divided into two subdomains, structural subdomain and functional subdomain. The structural subdomain mainly contains helices of A, G and H which are responsible for initial fast folding through hydrophobic core collapse. The other B−F helices are mainly for the binding of the prosthetic group heme with their polar amino acids and flexibility.

For the past decades, apoMb has served as an excellent model system for the study of protein-folding kinetics with a focus on hydrophobic collapses through various techniques,[58−62] especially nuclear magnetic resonance (NMR) in a great effort.[62] At pH6, apoMb is in native state and possesses ∼55% helical content while at pH4 the protein is partially folded and the helical percentage is ∼35%. Kinetic studies of apoMb folding persistently reveal the existence of an intermediate state which

(23) Lucent, D.; Vishal, V.; Pande, V. S. *Proc. Natl. Acad. Sci. U.S.A.* **2007**, *104*, 10430–10434.
(24) Papoian, G. A.; Ulander, J.; Eastwood, M. P.; Luthey-Schulten, Z.; Wolynes, P. G. *Proc. Natl. Acad. Sci. U.S.A.* **2004**, *101*, 3352–3357.
(25) Cruz, L.; Urbanc, B.; Borreguero, J. M.; Lazo, N. D.; Teplow, D. B.; Stanley, H. E. *Proc. Natl. Acad. Sci. U.S.A.* **2005**, *102*, 18258–18263.
(26) De Simone, A.; Dodson, G. G.; Verma, C. S.; Zagari, A.; Fraternali, F. *Proc. Natl. Acad. Sci. U.S.A.* **2005**, *102*, 7535–7540.
(27) Mukherjee, S.; Chowdhury, P.; Gai, F. *J. Phys. Chem. B* **2009**, *113*, 531–535. Mukherjee, S.; Chowdhury, P.; Gai, F. *J. Phys. Chem. B* **2007**, *111*, 4596–4602.
(28) Zhou, R.; Huang, X.; Margulis, C. J.; Berne, B. J. *Science* **2004**, *305*, 1605–1609.
(29) Billeter, M.; Guntert, P.; Luginbuhl, P.; Wuthrich, K. *Cell* **1996**, *85*, 1057–1065.
(30) Zhong, D.; Pal, S. K.; Zewail, A. H. *ChemPhysChem* **2001**, *2*, 219–227.
(31) Jayaram, B.; Jain, T. *Annu. Rev. Biophys. Biomol. Struct.* **2004**, *33*, 343–361.
(32) Zhong, D.; Douhal, A.; Zewail, A. H. *Proc. Natl. Acad. Sci. U.S.A.* **2000**, *97*, 14056–14061.
(33) Garczarek, F.; Gerwert, K. *Nature* **2006**, *439*, 109–112.
(34) Lin, J.; Balabin, I. A.; Beratan, D. N. *Science* **2005**, *310*, 1311–1313.
(35) Helms, V. *ChemPhysChem* **2007**, *8*, 23–33.
(36) Shrimpton, P.; Allemann, R. K. *Protein Sci.* **2002**, *11*, 1442–1451.
(37) Pocker, Y. *Cell. Mol. Life Sci.* **2000**, *57*, 1008–1017.
(38) Cohen, B. E.; McAnaney, T. B.; Park, E. S.; Jan, Y. N.; Boxer, S. G.; Jan, L. Y. *Science* **2002**, *296*, 1700–1703. Abbyad, P.; Shi, X. H.; Childs, W.; McAnaney, T. B.; Cohen, B. E.; Boxer, S. G. *J. Phys. Chem. B* **2007**, *111*, 8269–8276. Pierce, D. W.; Boxer, S. G. *J. Phys. Chem.* **1992**, *96*, 5560–5566. Abbyad, P.; Childs, W.; Shi, X. H.; Boxer, S. G. *Proc. Natl. Acad. Sci. U.S.A.* **2007**, *104*, 20189–20194.
(39) Ebbinghaus, S.; Kim, S. J.; Heyden, M.; Yu, X.; Heugen, U.; Gruebele, M.; Leitner, D. M.; Havenith, M. *Proc. Natl. Acad. Sci. U.S.A.* **2007**, *104*, 20749–20752. Ebbinghaus, S.; Kim, S. J.; Heyden, M.; Yu, X.; Gruebele, M.; Leitner, D. M.; Havenith, M. *J. Am. Chem. Soc.* **2008**, *130*, 2374–2375.
(40) Pal, S. K.; Peon, J.; Zewail, A. H. *Proc. Natl. Acad. Sci. U.S.A.* **2002**, *99*, 1763–1768. Peon, J.; Pal, S. K.; Zewail, A. H. *Proc. Natl. Acad. Sci. U.S.A.* **2002**, *99*, 10964–10969.
(41) Bashkin, J. S.; McLendon, G.; Mukamel, S.; Marohn, J. *J. Phys. Chem.* **1990**, *94*, 4757–4761. Riter, R. R.; Edington, M. D.; Beck, W. F. *J. Phys. Chem.* **1996**, *100*, 14198–14205.
(42) Jordanides, X. J.; Lang, M. J.; Song, X.; Fleming, G. R. *J. Phys. Chem. B* **1999**, *103*, 7995–8005.
(43) Changenet-Barret, P.; Choma, C. T.; Gooding, E. F.; DeGrado, W. F.; Hochstrasser, R. M. *J. Phys. Chem. B* **2000**, *104*, 9322–9329.
(44) Russo, D.; Hura, G.; Head-Gordon, T. *Biophys. J.,* **2004**, *86*, 1852–1862. Russo, D.; Murarka, R. K.; Copley, J. R. D.; Head-Gordon, T. *J. Phys. Chem. B* **2005**, *109*, 12966–12975. Johnson, M. E.; Malardier-Jugroot, C.; Murarka, R. K.; Head-Gordon, T. *J. Phys. Chem. B* **2009**, *113*, 4082–4092.
(45) Lu, W.; Kim, J.; Qiu, W.; Zhong, D. *Chem. Phys. Lett.* **2004**, *388*, 120–126.
(46) Zhang, L.; Kao, Y.-T.; Qiu, W.; Wang, L.; Zhong, D. *J. Phys. Chem. B* **2006**, *110*, 18097–18103.
(47) Qiu, W.; Li, T.; Zhang, L.; Yang, Y.; Kao, Y.-T.; Wang, L.; Zhong, D. *Chem. Phys.* **2008**, *350*, 154–164.
(48) Kim, J.; Lu, W.; Qiu, W.; Wang, L.; Caffrey, M.; Zhong, D. *J. Phys. Chem. B* **2006**, *110*, 21994–22000.
(49) Qiu, W.; Zhang, L.; Kao, Y.-T.; Lu, W.; Li, T.; Kim, J.; Sollenberger, G. M.; Wang, L.; Zhong, D. *J. Phys. Chem. B* **2005**, *109*, 16901–16910.
(50) Qiu, W.; Zhang, L.; Okobiah, O.; Yang, Y.; Wang, L.; Zhong, D.; Zewail, A. H. *J. Phys. Chem. B* **2006**, *110*, 10540–10549.
(51) Qiu, W.; Kao, Y.-T.; Zhang, L.; Yang, Y.; Wang, L.; Stites, W. E.; Zhong, D.; Zewail, A. H. *Proc. Natl. Acad. Sci. U.S.A.* **2006**, *103*, 13979–13984.
(52) Qiu, W.; Wang, L.; Lu, W.; Boechler, A.; Sanders, D. A. R.; Zhong, D. *Proc. Natl. Acad. Sci. U.S.A.* **2007**, *104*, 5366–5371.
(53) Zhang, L.; Wang, L.; Kao, Y.-T.; Qiu, W.; Yang, Y.; Okobiah, O.; Zhong, D. *Proc. Natl. Acad. Sci. U.S.A.* **2007**, *104*, 18461–18466.
(54) Phillips, S. E. V.; Schoenborn, B. P. *Nature* **1981**, *292*, 81–82.
(55) Jennings, P. A.; Wright, P. E. *Science* **1993**, *262*, 892–896. Eliezer, D.; Yao, J.; Dyson, H. J.; Wright, P. E. *Nat. Struct. Biol.* **1998**, *5*, 148–155.
(56) Hughson, F. M.; Barrick, D.; Baldwin, R. L. *Biochemistry* **1991**, *30*, 4113–4118. Hughson, F. M.; Wright, P. E.; Baldwin, R. L. *Science* **1990**, *249*, 1544–1548.
(57) Lecomte, J. T. J.; Sukits, S. F.; Bhattacharya, S.; Falzone, C. J. *Protein Sci.* **1999**, *8*, 1484–1491. Kim, Y. J.; Kim, Y. A.; Park, N.; Son, H. S.; Kim, K. S.; Hahn, J. H. *Biochemistry* **2005**, *44*, 7490–7496.

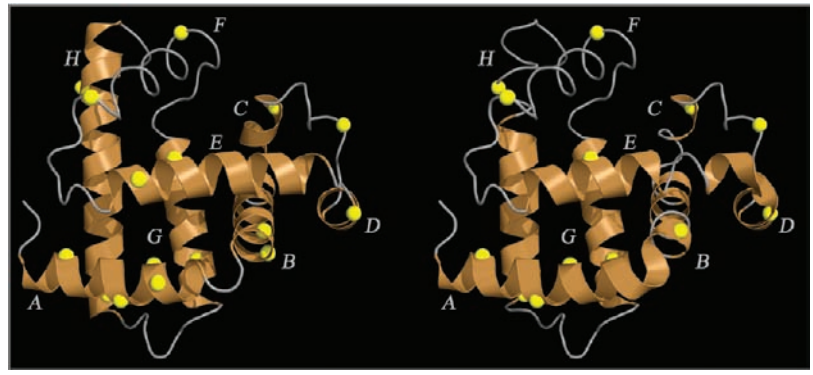

Figure 1. Mapping of hydration dynamics and water−protein fluctuations in two folding states of the helical apoMb. (*Left*) Structure of the native state of apoMb at pH6.[54] (*Right*) Structure of the molten globule state of apoMb at pH4 based on NMR studies.[55−57] The holoMb consists of eight helices, labeled as helices A−H. In apoMb, the frayed and flexible portions of the proteins are shown as thin loops, and the regions with stable helical structures are shown as ribbons. The mutation sites studied with the probe tryptophan are shown as yellow balls. Note the difference in contents and positions of secondary structures in the two states.

has the similar molten globular structure of the protein at pH4. Early events in folding mainly involve specific native-like interhelical hydrophobic contracts between helices A, G and H. Beside the hydrophobic A-G-H core, B and E helices are hypothesized to partially participate in early core formation. These studies mostly focused on interhelical interactions inside the protein, and the role of water was barely addressed.

In this work, by systematic studies of the relaxation dynamics around the surface of apoMb in two states using single optical probe tryptophan with femtosecond (fs) resolution, the water dynamics, their time scales and a series of dynamic correlations of water−protein fluctuations with local protein properties are determined. The changes of hydrogen-bond network in the hydration layer and local conformation flexibility in the probe proximity in different folding states (N and MG) are observed. These results reveal the intimate relationship of hydration dynamics with protein fluctuations and its folding structures.

Materials and Methods

Sample Preparation. The plasmid pMb122, containing sperm whale myoglobin gene, was generously provided by Sligar's group (University of Illinois at Urbana−Champaign).[63] Since the wild-type myoglobin has two intrinsic tryptophans, W7 and W14, we first examined the double mutation of W7YW14F, and the mutant was well overexpressed and stable, as also recently studied by the other group.[64] This double mutant was chosen as the triple mutation template. More than 30 triple mutants were designed based on the following considerations: (1) The replaced residue has no hydrogen bonding with neighboring residues to avoid a change of structure and stability;[65] (2) the replacing tryptophan is not in proximity of potential quenching residues such as histine and cysteine;[47,66] (3) the local topography is flat, concave or convex to examine geometric effects; (4) the local chemical identity is hydrophilic (polar or charged) or hydrophobic to examine electrostatic interactions;[67] (5) the distinct water residence times are selected for different mutated locations from recent MD simulations for all 297 hydration sites;[68] and (6) the structural stability of other mutants results from various previous studies.[69] Then, these mutants were carefully screened based on their folding structures by CD spectra and their stability and the fluorescence lifetimes. Finally, only 16 mutants were appropriate for study of hydration, and for each helix we have at least one mutant which has one tryptophan probe (Figure 1). These selected 16 mutants were then expressed in *Escherichia coli* in large quantity and purified with the methods described elsewhere.[63] The obtained pure holo protein solution was adjusted to pH2, and then the heme was removed by extraction three times with methylethylketone.[70] Then the solution was dialyzed against neutral deionized water for two times, each time 6 h to remove methylethylketone, and then two times against the buffer of 10 mM NaOAc at pH6 or 10 mM NaOAc at pH4, each time 6 h to bring the protein back to native (pH6) or molten globule state (pH4). CD spectra were double checked to make sure that all mutant proteins fold properly. The final protein was concentrated to 100−250 μM for femtosecond-resolved studies. All the steady-state fluorescence was measured using a SPEX FluoroMax-3 spectrometer. To ensure no change of the protein quality during data acquisition, we measured the protein fluorescence emission before and after each experiment. We also kept the sample in a rotating cell to minimize possible photobleaching or local heating.

Femtosecond-Resolved Fluorescence Up-Conversion Setup. All the femtosecond-resolved measurements were carried out using the femtosecond-resolved fluorescence up-conversion apparatus described elsewhere.[46,71] Briefly, the femtosecond pulse after the two-stage amplifier (Spitfire, Spectra-Physics) has a temporal width of 110 fs centered at 800 nm with a pulse energy of more than 2

(58) Uzawa, T.; Akiyama, S.; Kimura, T.; Takahashi, S.; Ishimori, K.; Morishima, I.; Fujisawa, T. *Proc. Natl. Acad. Sci. U.S.A.* **2004**, *101*, 1171–1176.
(59) Gilmanshin, R.; Williams, S.; Callender, R. H.; Woodruff, W. H.; Dyer, R. B. *Proc. Natl. Acad. Sci. U.S.A.* **1997**, *94*, 3709–3713. Gulotta, M.; Rogatsky, E.; Callender, R. H.; Dyer, R. B. *Biophys. J.* **2003**, *84*, 1909–1918.
(60) Abbruzzetti, S.; Crema, E.; Masino, L.; Vecli, A.; Viappiani, C.; Small, J. R.; Libertini, L. J.; Small, E. W. *Biophys. J.* **2000**, *78*, 405–415.
(61) Ballew, R. M.; Sabelko, J.; Gruebele, M. *Proc. Natl. Acad. Sci. U.S.A.* **1996**, *93*, 5759–5764.
(62) Eliezer, D.; Chung, J.; Dyson, H. J.; Wright, P. E. *Biochemistry* **2000**, *39*, 2894–2901.
(63) Springer, B. A.; Sligar, S. G. *Proc. Natl. Acad. Sci. U.S.A.* **1987**, *84*, 8961–8965.
(64) Sirangelo, I.; Tavassi, S.; Martelli, P. L.; Casadio, R.; Irace, G. *Eur. J. Biochem.* **2000**, *267*, 3937–3945.
(65) Hennig, M.; Geierstanger, B. H. *J. Am. Chem. Soc.* **1999**, *121*, 5123–5126.
(66) Chen, Y.; Barkley, M. D. *Biochemistry* **1998**, *37*, 9976–9982.
(67) Gu, W.; Schoenborn, B. P. *Proteins* **1995**, *22*, 20–26.
(68) Makarov, V. A.; Andrews, B. K.; Smith, P. E.; Pettitt, B. M. *Biophys. J.* **2000**, *79*, 2966–2974.
(69) Rohlfs, R. J.; Mathews, A. J.; Carver, T. E.; Olson, J. S.; Springer, B. A.; Egeberg, K. D.; Sligar, S. G. *J. Biol. Chem.* **1990**, *265*, 3168–3176. Egeberg, K. D.; Springer, B. A.; Sligar, S. G.; Carver, T. E.; Rohlfs, R. J.; Olson, J. S. *J. Biol. Chem.* **1990**, *265*, 11788–11795. Nguyen, B. D.; Zhao, X.; Vyas, K.; La Mar, G. N.; Lile, R. A.; Brucker, E. A.; Phillips, G. N., Jr.; Olson, J. S.; Wittenberg, J. B. *J. Biol. Chem.* **1998**, *273*, 9517–9526.
(70) Teale, F. W. J. *Biochim. Biophys. Acta* **1959**, *35*, 543–545.
(71) Saxena, C.; Sancar, A.; Zhong, D. *J. Phys. Chem. B* **2004**, *108*, 18026–18033.

mJ and a repetition rate of 1 kHz. Half of the laser energy was used to pump an optical parametric amplifier system (OPA-800C Spectra-Physics) to generate a 580-nm pulse. Then the pulse was frequency-doubled to generate the pump wavelength at 290 nm by a 0.2-mm-thick BBO crystal. The pump−pulse energy was typically attenuated to ∼140 nJ prior to being focused into the motor-controlled moving sample cell. The fluorescence emission was collected by a pair of parabolic mirrors and mixed with a gating pulse (800 nm) in another 0.2-mm BBO crystal through a noncollinear configuration. The up-converted signals ranging from 218 to 292 nm were detected. The instrument response time under this noncollinear geometry is between 400 and 500 fs as determined from the up-converted signal of Raman scattering by water at around 320 nm. For all hydration dynamics studies, the pump beam polarization was set at the magic angle (54.7°) with respect to the acceptable axis (vertical) of the up-conversion crystal. For local rigidity studies, the pump beam polarization was rotated to be either parallel or perpendicular to the acceptance axis to obtain the parallel ($I_{||}$) or perpendicular ($I_{\perp}$) signal, respectively.

Data Analyses. A series of wavelength-resolved fluorescence transients of tryptophan in the protein will be obtained for each mutant, and these transients usually show multiple exponential decays on the blue side and rise(s) at the red side of the emission peak. Although the fluorescence signals are from tryptophan emission, the decay and rise dynamics result from tryptophan's energy stabilization through local environment relaxation (water and/or the protein) and thus represent solvation dynamics.

With the method we have recently developed,[45] we are able to extract solvation response functions from the fluorescence transients of tryptophan. Briefly, all femtosecond-resolved fluorescence transients can be represented as a sum of two terms of discrete exponential functions

$$I_\lambda(t) = I_\lambda^{solv}(t) + I_\lambda^{popul}(t) = \sum_i \alpha_i e^{-t/\tau_i} + \sum_j \beta_j e^{-t/\tau_j} \quad (1)$$

where the first term associated with α_i and τ_i describes solvation processes and the second term associated with β_j and τ_j represents intrinsic lifetime emissions (population decays). The coefficient α_i is positive (decay dynamics) at the blue side of the emission peak and is negative (initial rise) at the red side. The coefficient β_j is always positive and represents relative contributions of lifetime emissions. Thus, the *overall* time-resolved emission spectra can be constructed as follows:

$$I(\lambda, t) = \frac{I_\lambda^{ss} I_\lambda(t)}{\sum_i \alpha_i \tau_i + \sum_j \beta_j \tau_j}, I(\nu, t) = \nu^{-2} I(\lambda, t) \quad (2)$$

where I_λ^{ss} is the relative steady-state emission intensity at wavelength λ. The time-resolved spectrum, after being converted to intensity versus frequency in cm^{-1}, was fitted to a log-normal function to deduce the emission maximum $\nu_s(t)$. Thus, a function of emission maxima with time can be obtained. In a similar manner, the time-resolved lifetime-associated emission spectra can also be constructed

$$I^{popul}(\lambda, t) = \frac{I_\lambda^{ss} I_\lambda^{popul}(t)}{\sum_i \alpha_i \tau_i + \sum_j \beta_j \tau_j}, I^{popul}(\nu, t) = \nu^{-2} I^{popul}(\lambda, t) \quad (3)$$

The emission maximum $\nu_l(t)$ is also deduced from a log-normal fit of the spectrum. By subtracting the lifetime-associated emission contribution $\nu_l(t)$ from the overall emission maximum $\nu_s(t)$, all derived solvation correlation functions can be constructed as follows:

$$c(t) = \frac{\nu_s(t) - \nu_l(t)}{\nu_s(0) - \nu_l(0)} \quad (4)$$

These solvation correlation functions often follow a robust double-exponential decay,

$$c(t) = a_1 e^{-t/\tau_1} + (1 - a_1) e^{-t/\tau_2} \quad (5)$$

Importantly, for the two time constants of τ_1 and τ_2, the corresponding solvation energies, ΔE_1 and ΔE_2, from the total Stokes shift, $\Delta E = \Delta E_1 + \Delta E_2 = \nu_s(0) - \nu_l(0)$, are also derived. Thus, we can define an average solvation speed (or an average solvent reorganization rate) to express how much energy drop (in cm^{-1}) per picosecond by local polarization changes.

$$S_1 = \frac{\Delta E_1}{\tau_1},\ S_2 = \frac{\Delta E_2}{\tau_2} \quad (6)$$

The two variables (S_1 and S_2) directly reflect how quickly the local environment responds to the external perturbation by sudden changes of static dipole moments through optical excitation and are related to the flexibility of their solvation contributors, mostly the H-bond water networks.

For examination of the probe's rigidity, we can obtain parallel ($I_{||}$) and perpendicular ($I_{\perp}$) fluorescence signals to construct anisotropy changes (r) with time, which represents femtosecond-resolved rotational dynamics,

$$r(t) = \frac{I_{||}(t) - I_{\perp}(t)}{I_{||}(t) + 2I_{\perp}(t)} \quad (7)$$

Typically, the obtained anisotropy dynamics are well fitted by several exponential decays, and the total anisotropy is usually expressed by a sum of three parts: $r(t) = r_I + r_W + r_T$. The initial ultrafast decay (r_I) in about 100 fs results from internal conversion between the two electronically excited states of ^1L_a and ^1L_b, as observed before.[72,73] The anisotropy for all transients initially drops to a value of ∼0.12 in such a short time and this *apparent* anisotropy ($r_{app} = r_W + r_T \sim 0.12$) is consistent with the early reported value at excitation of 290 nm.[74] The second component (r_W) represents the local wobbling motion of the tryptophan probe in time τ_w, which reflects the local packing and backbone rigidity. The last term r_T is the global tumbling motion of the entire protein, and the time scale was about ∼10 ns. The key term here is r_W and the corresponding time scale of τ_w. The wobbling semi-angle (θ) can be estimated using the model of an axially symmetric oscillation about a fixed axis,[75] giving the expression:

$$1 - \frac{r_W}{r_{app}} = \left[\frac{3\cos^2\theta - 1}{2}\right]^2 \quad (8)$$

Accordingly, for the derived semi-angle θ, we can define an average wobbling angular speed ω, which represents how fast the probe can wobble in the constrained angle θ.

$$\omega = \frac{\theta}{\tau_w} \quad (9)$$

Results

Femtosecond-Resolved Fluorescence Transient Dynamics. Figure 2 shows the femtosecond-resolved fluorescence transients of mutant A71W in two states for several typical wavelengths from the blue to red side. The steady-state fluorescence emission peaks of A71W are 337 nm at pH6 and 336 nm at pH4. More than 10 emission wavelengths are gated for each mutant from the blue to red side of the emission peak within 3-ns time

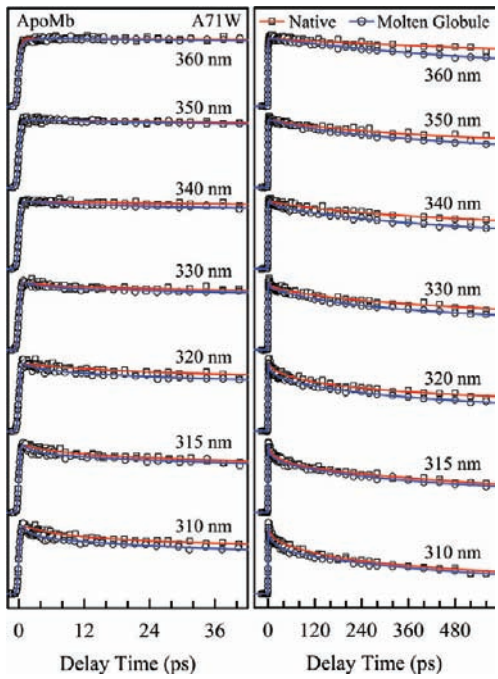

Figure 2. Normalized femtosecond-resolved fluorescence transients of mutant A71W with a series of wavelength detection in native (red) and molten globule (blue) states in short (*Left*) and long (*Right*) time ranges. The squares and circles are the experimental data, and the solid lines are the best multiple-exponential fit.

window. The overall decay times in both states are significantly slower than those of Trp in water.[45] A global fitting strategy was employed to fit all the transients. Four exponential functions are sufficient to well fit all the transients, and two of the exponentials are constant lifetime decays. The fitting results using eq 1 for both states are given in Table 1S in the Supporting Information.

For the mutants we studied, the lifetimes were found by fitting the red-side transients, typically at 350−380 nm, with two exponential decays and one or two ultrafast rise components, if necessary. For A71W in the Figure 2, the lifetimes were found to be 680 ps and 7.95 ns at pH6, and 420 ps and 3.1 ns at pH4. The shorter lifetimes at the molten globule state, mostly resulting from the electron-transfer quenching by neighboring peptide amide bond(s),[76] indicate a more flexible local protein environment around the tryptophan than at the native state. This observation is general for nearly all other mutants. Besides lifetime contributions, solvation components for all blue-side transients are well represented by a double-exponential decay, which gradually slows down toward the longer emissions, and becomes a fast initial rise at red side (Figure 2). This pattern is a typical behavior of local solvation dynamics.[77,78] For example, in A71W, the two solvation components decay at pH6 in 2.2−9.9 ps and 58−71 ps from the blue side toward the emission peak and at pH4 these times become to 2−5.2 ps and 34−45 ps. The time scales in the molten globule state are faster than in the native state for all mutants studied except one mutant A57W, but they are all much slower in both states than tryptophan in bulk water,[45] suggesting more constraints for local relaxation. Globally, the observed time scales of solvation dynamics are very different for different mutants and states, strongly depending on local protein properties, as will be discussed below.

Solvation Correlation Functions and Two Time Scales. Figure 3 shows a 3D representation of constructed femtosecond-resolved emission spectra (FRES) for mutant A71W in two states using eqs 2 and 3 and the resulting emission maxima of $\nu_s(t)$ and $\nu_l(t)$ with time. A−C of Figure 3 are for the native state and D−F are for the molten-globule state. Using eq 4, we can obtain the total Stokes shift $\nu_s(0) - \nu_l(0)$ and derive the solvation correlation function $c(t)$. Figure 4 shows the final correlation functions of all 16 mutants in native and molten globule states, along with their local structures and chemical properties in 12 Å. Strikingly, all solvation correlation functions can be robustly fitted by double exponential decays with two time constants using eq 5. One is in a few picoseconds, and the other ranges from tens to hundreds of picoseconds. The fitting time constants and the corresponding percentages of all mutants, along with their fitting lifetimes, total (ΔE) and two separated (ΔE_1 and ΔE_2) Stokes shifts and initial ($t = 0$) and measured steady-state emission peaks, are given in Table 2S in the Supporting Information.

The observed two time scales in the correlation functions are the responses of local environment on the sudden dipole changes of Trp upon excitation. In principle, these responses can result from surrounding hydration water molecules and protein side chains and backbone. However, in our recent solvation studies on enzyme *Staphylococcus* nuclease[51] and human thioredoxin,[52] we found that mutations of charged and polar residues around Trp into nonpolar amino acids have minor effects on the total Stokes shifts and solvation dynamics. With further demonstration in our recent MD simulations on W7 in myoglobin,[79] we assigned the two time scales to two kinds of water-network motions: local collective water-network relaxation and subsequent water-network restructuring, coupled with protein fluctuations. Here, *any hydrating water motions, coupled or decoupled with protein fluctuations, are an integral part of the hydration dynamics and thus are all referred as hydration dynamics.* Hence, the observed 29 solvation correlation functions mainly represent the local hydration dynamics at 16 specific sites among A-H helices in two states around the protein surface.

Overall, among 16 mutants in Figure 4, most mutants except A57W show the slower hydration dynamics in N state than in MG state. Specifically, the hydration dynamics of eight mutants on two time scales, W7 (5.0/87 ps in N state and 3.5/73 ps in MG state), H12W (5.1/99 ps and 3.1/77 ps), W14 (8.2/103 ps and 4.5/76 ps), A22W (2.9/60 ps and 1.0/61 ps), E41W (6.3/192 ps and 2.9/144 ps), A71W (3.8/58 ps and 2.5/41 ps), A84W (2.2/38 ps and 1.3/35 ps) and T95W (1.8/24 ps and 1.1/22 ps), all show some longer relaxations in N state with more difference for the first components. However, another four mutants, H48W (1.3/44 ps and 0.7/21 ps), H113W (2.8/69 ps and 1.8/26 ps), A127W (5.7/50 ps and 1.7/32 ps) and A144W (5.5/209 ps and

(72) Zhong, D.; Pal, S. K.; Zhang, D.; Chan, S. I.; Zewail, A. H. *Proc. Natl. Acad. Sci. U.S.A.* **2002**, *99*, 13–18.
(73) Shen, X.; Knutson, J. R. *J. Phys. Chem. B* **2001**, *105*, 6260–6265.
(74) Valeur, B.; Weber, G. *Photochem. Photobiol.* **1977**, *25*, 441–444.
(75) Steiner, R. F. In *Topics in Fluorescence Spectroscopy*; Lakowicz, J. R., Ed.; Plenum: New York, 1991; Vol.2, pp 1−51.
(76) Callis, P. R.; Liu, T. *J. Phys. Chem. B* **2004**, *108*, 4248–4259.
(77) Jarzeba, W.; Walker, G. C.; Johnson, A. E.; Kahlow, M. A.; Barbara, P. F. *J. Phys. Chem.* **1988**, *92*, 7039–7041.
(78) Jimenez, R.; Fleming, G. R.; Kumar, P. V.; Maroncelli, M. *Nature* **1994**, *369*, 471–473. Horng, M. L.; Gardecki, J. A.; Papazyan, A.; Maroncelli, M. *J. Phys. Chem.* **1995**, *99*, 17311–17337.
(79) Li, T.; Hassanali, A. A.; Kao, Y.-T.; Zhong, D.; Singer, S. J. *J. Am. Chem. Soc.* **2007**, *129*, 3376–3382. Li, T.; Hassanali, A. A.; Singer, S. J. *J. Phys. Chem. B* **2008**, *112*, 16121–16134.

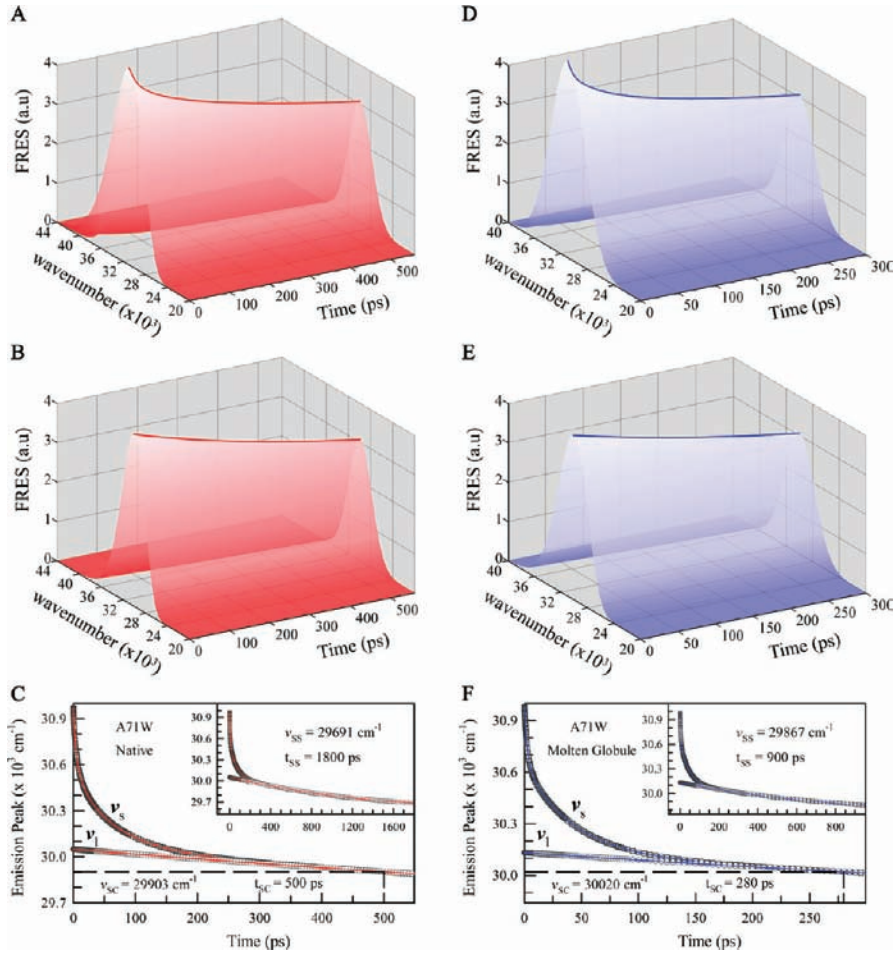

Figure 3. Femtosecond-resolved emission spectra (FRES) of mutant A71W in native (A−C, red) and molten globule (D−F, blue) states. (*Top: A and D*) 3D representation of the evolution of the *overall* FRES. (*Middle:B and E*) 3D representation of the evolution of the *lifetime-associated* FRES. (*Bottom: C and F*) Temporal evolution of the emission peaks of overall (ν_s) and lifetime-associated (ν_l) FRES. The inset shows ν_s and ν_l until they reach the steady-state emission peaks (ν_{ss}) at t_{ss}.

3.2/53 ps), have the significantly different hydration dynamics in two states. For A57W (1.4/24 ps and 1.7/48 ps), we observed the similar first components but very different second components and the hydration dynamics are slower in MG state. Three other mutants, A15W (5.6/92 ps), G23W (7.2/133 ps) and A74W (4.0/150 ps), were only studied in N state, not MG state, due to the extremely low protein expression yields.

The resulting total Stokes shifts and the corresponding two separated components are shown in Figure 5. The total Stokes shifts (487−2203 cm^{-1}) show a monotonic increase with the emission maxima and can be fit with a quadratic function of λ (nm) in the range from 326.9 to 349.7 nm, i.e., ΔE (cm^{-1}) = $214633.8-1337.5\lambda + 2.1\lambda^2$, as shown in Figure 5B. The first-component Stokes shifts (ΔE_1) also show a quadratic function (Figure 5D), but the second components (ΔE_2) strikingly follow a sigmoidal function, reaching a plateau when the emission maxima are longer than 338 nm (Figure 5C). The corresponding two time scales (τ_1 and τ_2) of the hydration dynamics for all 16 mutants in two states are shown in Figure 6. These extensive experimental data and derived various correlations between the hydration dynamics with local protein properties will be discussed below.

Anisotropy Dynamics and Wobbling Rotational Motions. Figure 7 shows femtosecond-resolved anisotropy dynamics of mutant A84W by gating wavelengths typically around emission peaks. The resulting r(t) using eq 7 clearly shows three typical relaxations of the probe Trp in the proteins: initial electronic relaxation (r_I) around 100 fs, local Trp wobbling rotational motion (r_W) in 55 ps in N state and 69 ps in MG state, and entire protein tumbling motion (r_T) in about 10 ns. Here, we focus on the local Trp wobbling rotational motions in all mutants. Using eqs 8 and 9, we obtained the wobbling semi angles of 14.2° and 16.2° and the angular speeds of 0.26°/ps and 0.23°/ps for N and MG states, respectively. For all 14 mutants studied, the apparent anisotropies (r_{app}) after initial ultrafast electronic relaxation are around 0.12 and the resulting wobbling angles, time scales, and angular speeds are all given in Table 3S in the Supporting Information and mostly shown in Figure 8. Globally, the wobbling rotational semi angles of the probe tryptophan range from 11.7° (H113W in N state) to 27° (A57W in N state) with most about 17° (Figure 8A). The local rotational time scales range from tens to hundreds of picoseconds. Among 14 mutants studied, two mutants T95W (N and MG) and A144W (MG) in very loose loop regions (Figure 1) show two wobbling rotational motions with similar time scales of ∼12 and 382 ps for both N and MG states of T95W (not shown in Figure 8) and 60 and 800 ps for MG state of A144W. The first rotational relaxation is apparently from the local Trp wobbling motion and the second relaxation represents the loose loop motion, but these two motions are obviously coupled. For all other mutants, the observed various

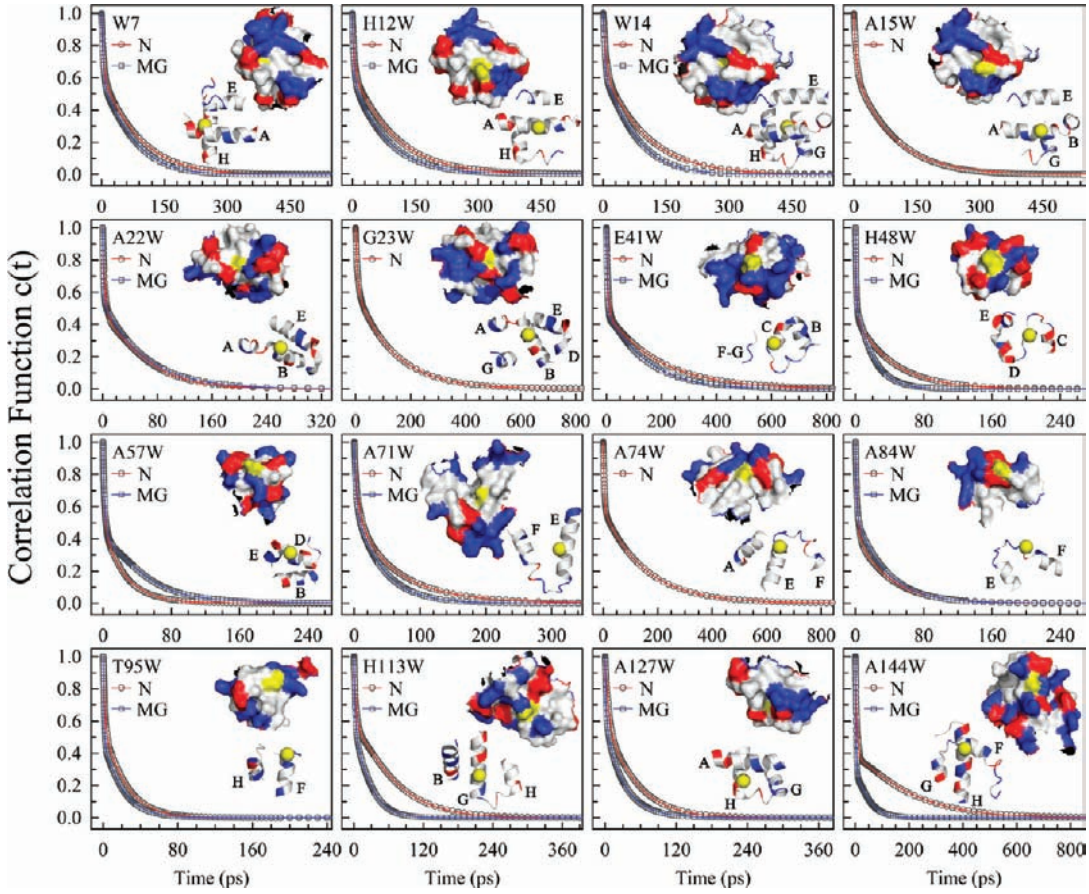

Figure 4. Hydration correlation function $c(t)$ of 16 mutants in both native (N, red) and molten globule (MG, blue) states. The solid lines are the best biexponential fit to $c(t)$. The insets show the local protein environments around the mutation sites in about 12 Å in surface map and ribbon representation. On surface maps, white, blue and red colors represent nonpolar, positively and negatively charged residues, respectively, and mutation sites are in yellow. On ribbon structures, mutation sites are indicated with yellow balls and the A−H letters indicate the identities of local helices. For mutants of A15W, G23W and A74W, only the native state was studied. For H12W and A15W, the A-helix was rotated, and the tryptophan was buried inside the protein.

correlations of local flexibility with protein properties in Figure 8 will be discussed below.

Discussion

The Origin of Two Dynamic Stokes Shifts (ΔE_1 and ΔE_2). Figure 5B−D shows the total dynamic Stokes shifts and the individual contributions ΔE_1 and ΔE_2 from the two hydration relaxations, τ_1 and τ_2, respectively, of all 16 mutants in two states with increase of Trp fluorescence emission peaks (λ_{max}). The two Stokes shifts of ΔE_1 and ΔE_2 display distinct relationships with λ_{max}: ΔE_1 increases monotonically from 180 to 1600 cm^{-1}; ΔE_2 increases gradually from initial 340 cm^{-1} and reaches a plateau about 650 cm^{-1} at 338 nm. According to the observed trend of ΔE_2, we can divide the emission peaks into three regions: (I) $\lambda_{max} \leq 330$ nm; (II) 330 nm $< \lambda_{max} <$ 338 nm; and (III) $\lambda_{max} \geq 338$ nm. Surprisingly, these three regions are well correlated with Trp locations relative to protein surfaces from buried below 330 nm, to partially buried at 330−338 nm and to exposed to solvent at the protein surface above 338 nm (Figure 5).[80] Using Trp as a local probe, we can detect neighboring water molecules within a distance of, at least, ∼10 Å.[39,40,81] Thus, the results show that ΔE_1 is clearly related to the extent of Trp exposure and directly proportional to total amount of relaxing water molecules. However, ΔE_2 is only related to hydrating water molecules in the inner shell at the water−protein interface. As shown in Figure 5C and D, as long as the probe moves to the protein surface, ΔE_2 is about constant and all interfacial water relaxation is completely detected, while ΔE_1 displays an accelerated increase and more mobile hydration water relaxation when the outer layer is probed. When the probe is buried and away from the protein surface, we detected less hydration water molecules, and hence both ΔE_1 and ΔE_2 become smaller. Figure 5A exactly shows such direct correlation between ΔE_1 and ΔE_2. Below 338 nm, ΔE_1 shows a linear relationship with ΔE_2, indicating that both relaxations of ΔE_1 and ΔE_2 are from the same number of water molecules in the inner hydration shell. Above 338 nm, ΔE_1 keeps increasing, while ΔE_2 is nearly constant.

These observations are striking, and the observed ∼650 cm^{-1} Stokes shift at the protein surface, nearly independent of local protein properties, must reflect the nature of interfacial hydrating water molecules. With different topological roughness and chemical property around the surface, ΔE_2 only fluctuates within ±75 cm^{-1}, about 12% of the relaxation energy of ΔE_2. This observation clearly indicates that ΔE_2 is not mainly from the contributions of protein solvation, especially the neighboring charged residues as predicted by MD simulations.[82−84] For

(80) *Principles of fluorescence spectroscopy*; Lakowicz, J. R., Ed.; Springer: New York, 2006.
(81) Finney, J. L. *Faraday Discuss.* **1996**, *103*, 1–18.
(82) Vivian, J. T.; Callis, P. R. *Biophys. J.* **2001**, *80*, 2093–2109.
(83) Golosov, A. A.; Karplus, M. *J. Phys. Chem. B* **2007**, *111*, 1482–1490.

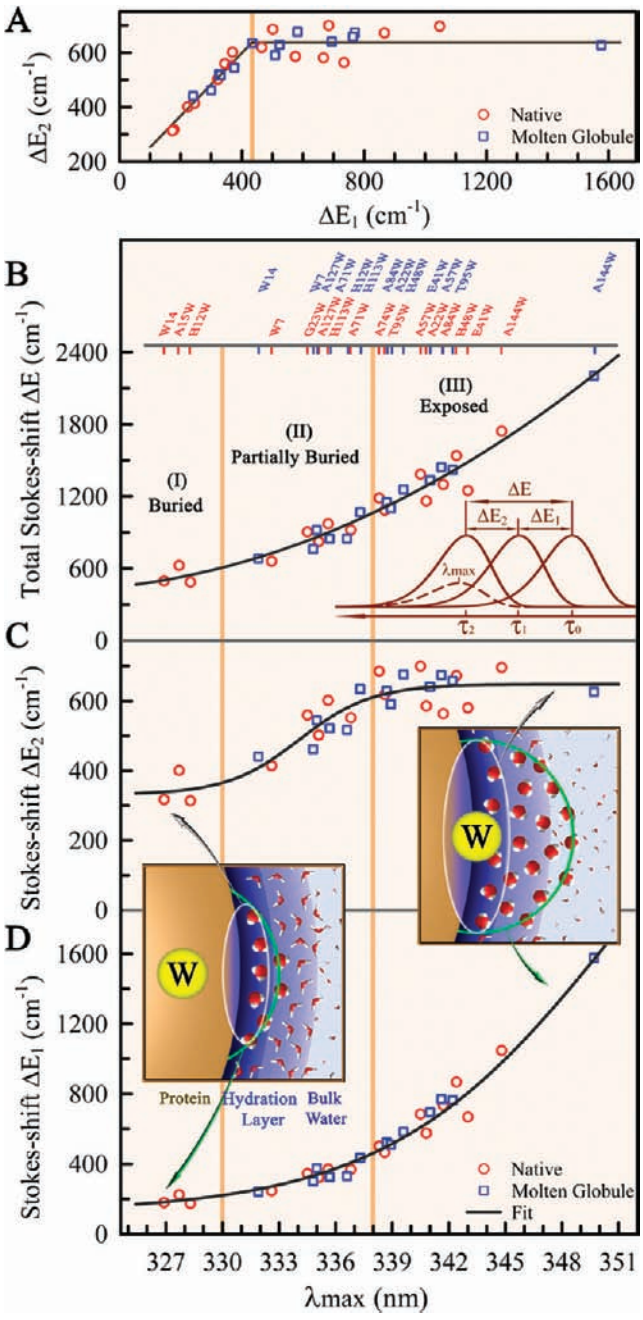

Figure 5. Dynamic Stokes shifts of all 16 mutants in two states. Red circles (N) and blue squares (MG) are the original data, and the black lines show the changing trends. (A) Correlation between the two Stokes shifts ΔE_1 and ΔE_2. The vertical yellow bar corresponds to ΔE_1 of 460 cm^{-1} and λ_{max} of 338 nm in (D). (B−D) Correlations between the Stokes shifts and steady-state emission peaks λ_{max}. The two vertical yellow bars divide λ_{max} into three regions of tryptophan locations. All mutants are shown on the top in (B) and the ticks correspond to the data points below. The inset in (B) shows the physical meaning of two separated Stokes shifts with two distinct times relative to the steady-state emission in dashed line. The insets in (C,D) show different contributions of surface hydration waters to ΔE_1 (green arcs and arrows) and ΔE_2 (white ellipses and gray arrows) when tryptophan is buried (left) or exposed (right). Water molecules in big arcs are within ∼10 Å around tryptophan and waters in small ellipses are those directly interacting with the protein at the water−protein interface and probed by tryptophan.

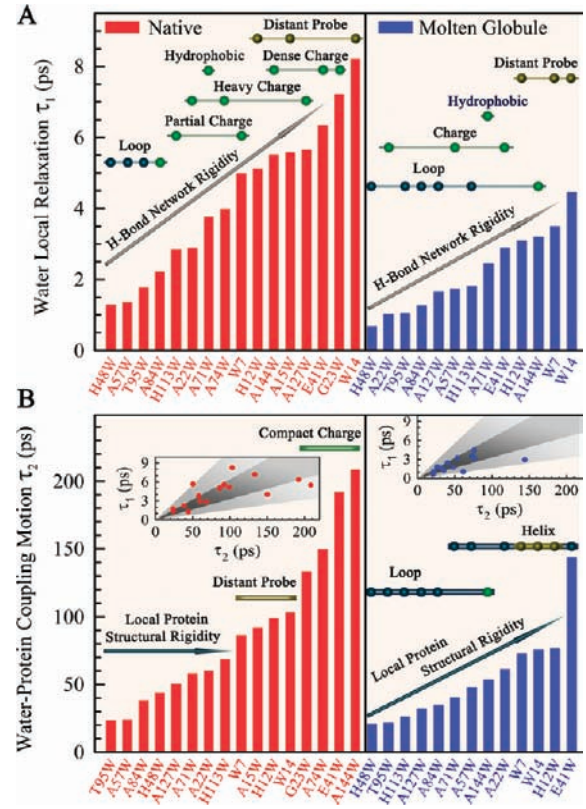

Figure 6. Time scales of two water-network relaxations τ_1 (A) and τ_2 (B) of 16 mutants in N (*left*) and MG (*right*) states. In each panel, above the bars are the classification of mutation sites, divided according to their secondary structure (dark blue), charge distribution (green) and probe location (yellow). The beads correspond to the data below them. The insets in (B) show the correlation between the two water-network dynamics in each state. Note the significant differences of these two water-network dynamics in N and MG states and the heterogeneous distributions of the time sales at different sites.

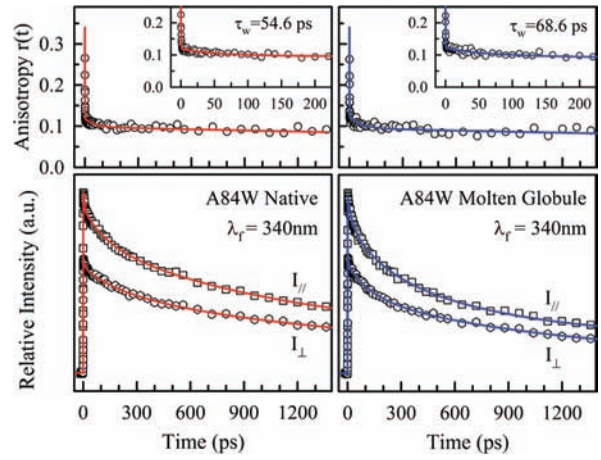

Figure 7. Construction of fluorescence anisotropic dynamics of tryptophan residues in representative mutant A84W in both native and molten globule states. Fluorescence transients were gated around the emission peak of 340 nm under parallel ($I_{||}$) and perpendicular ($I_{\perp}$) conditions. The resulting anisotropy dynamics, $r(t)$, are shown in top panels, and the insets show the short-time behaviors.

example, T95W and A144W have very different charge distributions around Trp (Figure 4) but give similar ΔE_2 values. Thus, ΔE_2 is dominantly from the contributions of hydrating water molecules in the inner layer, and our results are drastically different from the MD prediction.[82,84] The nearly constant value at the protein surface indicates that all lateral interfacial water molecules within the probed range (∼10 Å) can completely relax with a similar water density at different Trp locations around

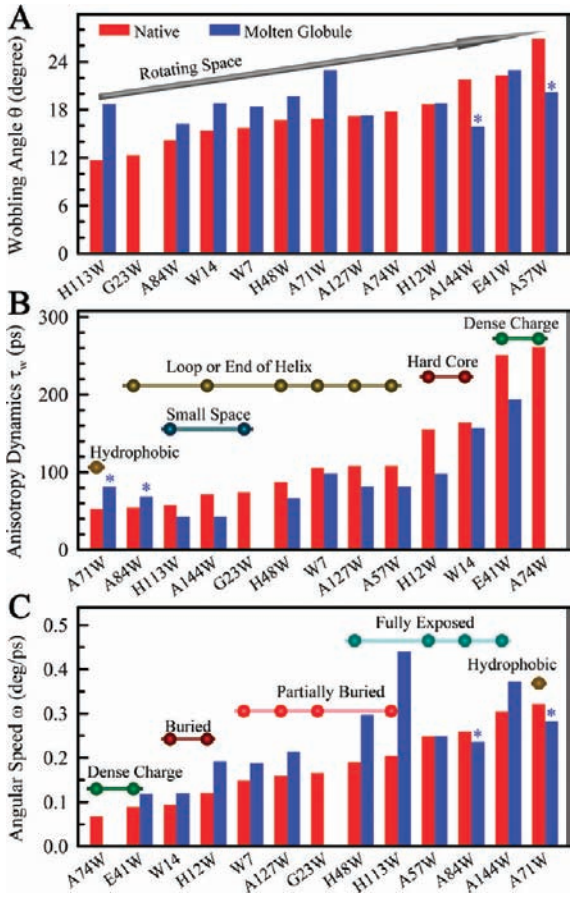

Figure 8. Correlations of tryptophan's rotational motion with local protein properties for both native (red) and molten globule (blue) states. Tryptophan rotational motion is characterized with physical parameters of wobbling angle (A), rotational time (B), and angular speed (C). Each parameter shows certain correlation with local protein properties around tryptophan, and mutants marked with asterisks are special cases (see text).

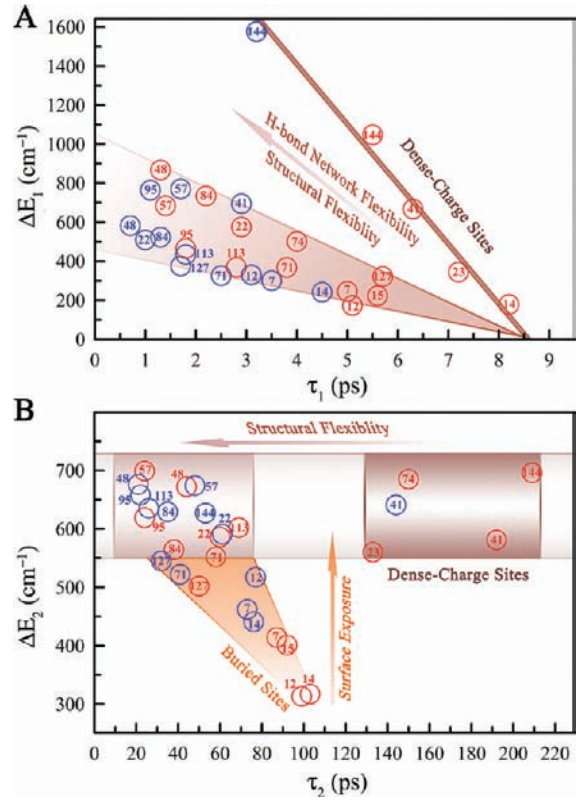

Figure 9. Correlations of dynamic Stokes shifts with the corresponding hydration dynamics. The red and blue circles are the data points of native and molten globule states, respectively. Each data point is labeled with its residue number of mutation site. (A) ΔE_1 and τ_1 show a simple correlation based on H-bond water-network flexibility and structural flexibility. Dense-charged sites deviate from the general trend and show a smooth linear correlation of ΔE_1 and τ_1. (B) Plot of ΔE_2 and τ_2 shows three distinct regions because of different local properties around tryptophan with no direct correlations. Overall it shows general dependence on surface exposure and structural flexibility as indicated by arrows.

the surface and must reflect the unique property of H-bond water networks in the inner hydration layer.

The Nature of Two Distinct Water Motions (τ_1 and τ_2). The stabilization energy of the Stokes shifts above was found to come from the dominant hydrating water relaxations, but the relaxation dynamics and time scales are directly related to local protein structural and chemical properties. As shown in Figure 6A, the initial water relaxation (τ_1) occurs in 1.3−8.2 ps in N state and in 0.7−4.5 ps in MG state for H48W and W14, respectively, and the time scales are all in a few picoseconds. Very surprisingly, we did not observe the relaxation on the femtosecond time scale as did in bulk solution[45,77,78] and the femtosecond relaxation of hindered motions greatly slows down. *This result shows that the H-bond water network in the hydration layer is much more rigid than in bulk water and the relaxation in a few picoseconds must be from local collective water-network motions.* Because we observed the shortest time to be 0.7 ps for H48W in MG state, still much longer than bulk-water relaxation, the probed relaxation water is not bulklike yet. Also, the probe is already exposed at the protein surface; thus, we concluded that the hydration layer probably extends to more than 10 Å from the protein surface, consistent with recent THz studies.[39] In Figure 9A, we show the relationship of the relaxation energy (ΔE_1) and its time (τ_1). Overall, the stabilization energy increases and the relaxation time decreases, consistent with Figure 5 and indicating that, when Trp moves to the protein surface, more outer-layer water molecules are probed and also these water molecules relax relatively faster. These collective water-network motions are clearly related to local chemical property and structural integrity of the protein, as well as the probe locations.

Specifically, in N state (Figure 6A) we observed: (i) In loop regions (H48W, A57W, T95W and A84W), the dynamics occur fastest in 1.3−2.2 ps, consistent with more flexible H-bond networks around lower-order structures, resulting in fast relaxation; (ii) for charge environments, the relaxation dynamics take from 2.8 ps (H113W) to 7.2 ps (G23W) for partial- to dense-charged surroundings (Figure 4). Clearly, in the dense-charged areas (A144W, E41W and G23W) the relaxations are longest, and a linear correlation of ΔE_1 with τ_1 was observed (Figure 9A); (iii) for the hydrophobic site of A71W, the initial water motion occurs in 3.8 ps, slower than those in loop regions and probably resulting from the collective water-ring structure relaxation at the hydrophobic site;[85,86] (iv) for three buried sites (H12W, A15W and W14), the distances from the probe to the protein surface are longer, and the forces on relaxing water

(84) Nilsson, L.; Halle, B. *Proc. Natl. Acad. Sci. U.S.A.* **2005**, *102*, 13867–13872.
(85) Smolin, N.; Winter, R. *J. Phys. Chem. B* **2004**, *108*, 15928–15937.
(86) Ruan, C.-Y.; Lobastov, V. A.; Vigliotti, F.; Chen, S.; Zewail, A. H. *Science* **2004**, *304*, 80–84. Yang, D.-S.; Zewail, A. H. *Proc. Natl. Acad. Sci. U.S.A.* **2009**, *106*, 4122–4126.

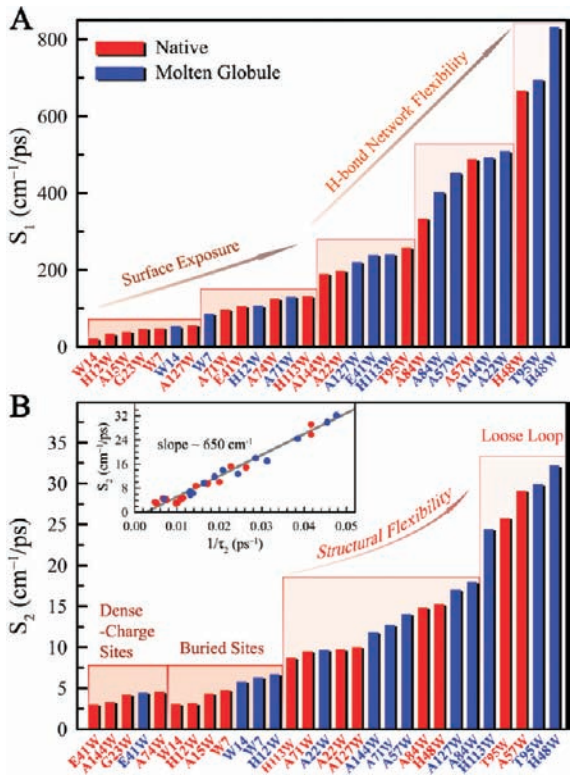

Figure 10. Hydration speed (S_1 and S_2) representation of water-network dynamics of all mutants studied. (A) Initial fast local collective relaxation S_1. S_1 generally increases with more surface exposure and H-bond network flexibility. (B) Subsequent slow water-network restructuring S_2. S_2 is slow around dense-charged sites and buried sites, and increases with increasing of local protein structural flexibility. The inset in (B) shows a predominant linear dependence of S_2 on $1/\tau_2$.

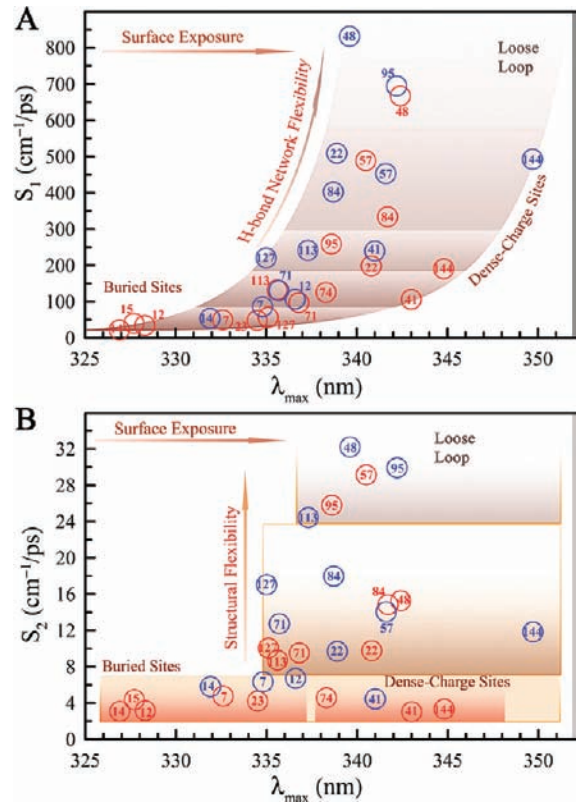

Figure 11. Correlations between hydration speeds of water networks and emission peaks of tryptophan residues for both native (red) and molten globule (blue) states. (A) S_1 is strongly correlated with tryptophan surface exposure and H-bond water-network flexibility. (B) Besides surface exposure, S_2 also strongly depends on local protein structural flexibility. In both (A) and (B), layers of shades emphasize that mutants with similar properties (i.e., surface exposure, structural flexibility, and local chemical identity) have similar hydration speeds and dense-charged sites slow down both S_1 and S_2.

molecules would be weaker. We observed the longest relaxation dynamics around 6−8 ps and especially for the most buried W14, the distance to the protein surface is about 7 Å and the dynamics is already falling on the dense-charged trend (Figure 9A); and (v) for MG state, the observed correlations are similar as in N state and all water motions except A57W become faster (Figure 6), strongly indicating that the H-bond water networks around the protein globally become weaker and more mobile due to the loose and bigger MG structure as observed by others. For A57W, the probe in N state is near a loop region, but in MG state, the probe region becomes a part of a helix (Figure 1), as observed from the fluorescence emission (Figure 5), rotational anisotropy (Figure 8A) and NMR studies.[62] These results strongly indicate that in MG state, the hydration water networks at many sites are not fully developed as shown here from emission peaks, Stokes shifts, and the relaxation dynamics (also see τ_2 below), supporting the current hypothesis that water could be finally squeezed out when the protein collectively folds into the final tertiary structure.[4,61]

The dynamics of the second relaxation (τ_2) take much longer times, and the time scales cover a wide range from 24 ps (T95W) to 209 ps (A144W) in N state and 21 ps (H48W) to 144 ps (E41W) in MG state. This longer relaxation represents the interactions of the interfacial water molecules in the inner hydration shell with the local protein and directly reflects the dynamics of water−protein fluctuations. As reported by our recent MD simulations (also see below),[79] by freezing either the protein or hydration water, the longer relaxation would disappear. From the energy relaxation of ΔE_2, we know that the relaxation is dominated by the inner hydration layer of water.

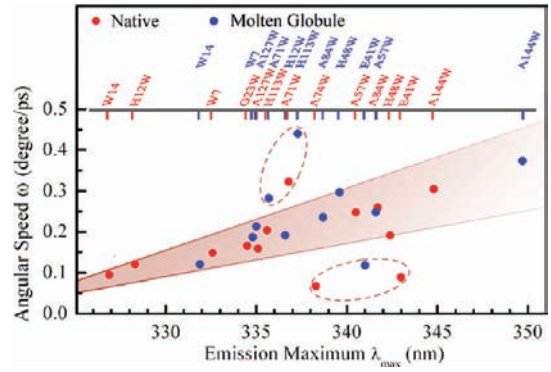

Figure 12. Correlations between the angular speed ω of tryptophan wobbling motion and its steady-state emission peak λ_{max}. All mutants studied are shown on the top, and the ticks correspond to the filled circles below. The angular speed ω increases with increasing λ_{max}, well correlated with the probe's locations from buried inside the protein to fully exposed to the surface. Data in dashed circles are special cases (see text).

Upon the sudden change of dipole moments of the probe, after the initial relaxation, the water networks need restructuring around the new dipole moment of the probe. Such a large rearrangement requires local protein fluctuations and is also facilitated by dynamic exchange with outside bulk water. These interactions are coupled, and the motions are collective. Although the entire relaxation energy of the inner hydration-layer water only fluctuates within 12%, clearly the dynamics is

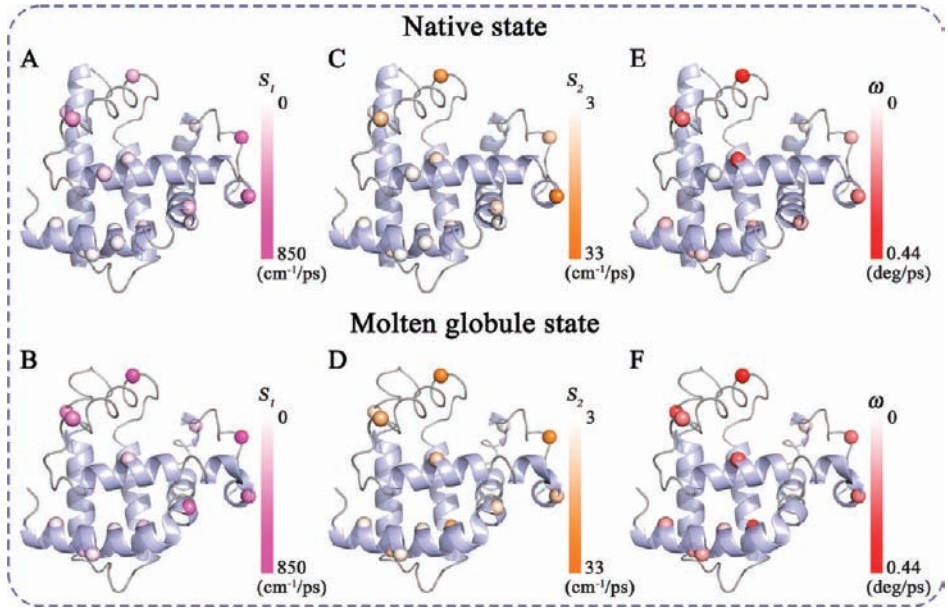

Figure 13. Color scale representation of hydration dynamics (S_1 and S_2), water−protein fluctuations (S_2) and local protein wobbling motions (ω) at 16 positions of apoMb in native (*top*) and molten globule (*bottom*) states. The mutant sites are shown in balls, and the colors of the balls are scaled linearly, with light colors for slow dynamics and dark colors for fast dynamics. Note the difference in contents and positions of secondary structures and colors of balls in two states.

coupled to protein fluctuations and tightly related to protein properties as shown in Figure 6B.

Specifically, we observed in N state: (i) For the mutants from T95W to H113W, the dynamics are well correlated with the local protein structural rigidity, i.e., tertiary interactions and these relaxations occur within 70 ps. Because the protein is more flexible in loop regions, the coupled water−protein relaxation is fastest for the loop probe T95W, A57W, A84W and H48W; (ii) for four compact charged probe sites of G23W, A74W, E41W and A114W, the hydrating water relaxation is slowest in 133−206 ps, a similar behavior observed in τ_1; (iii) for four buried probe sites of W7, A15W, H12W and W14 in A helix, they show all similar relaxation times of 87−103 ps, supporting that the dynamics represents the local coupled motion of the inner hydration water network with A-helix. The slightly longer relaxation time also results from the weaker perturbation induced by the buried distant probe; (iv) For MG state, except A57W all the dynamics become faster, indicating a loose MG structure. Indeed, partial helices already become loose loops and the helices become more flexible due to the loss of higher-order structures. These observed correlations are shown in Figure 9B in the relationship of ΔE_2 with τ_2. Clearly, the dense-charged sites show distinct dynamical behaviors, and the chemical identities of the local protein play a critical role.[44]

The correlations of τ_2 and τ_1 in Figure 6B for N and MG states show the intrinsic connection of two water relaxations. Generally, the slower the initial water relaxation, the longer time the water-network restructuring takes. The dynamics are convoluted with protein chemical properties (τ_2 and τ_1) and higher-order structure (mainly τ_2). Thus, in N state, the correlation is more diverse; the mutants with dense-charged surroundings show longer τ_2, and the mutants with distant probe locations give longer τ_1. However, in MG state, since the protein has more loop regions and the structure becomes more flexible, the τ_2 and τ_1 become well correlated, showing nearly a straight line except a few dense-charged sites and indicating that the dynamics are less dependent on the protein structures and dominated by the hydrating water networks.

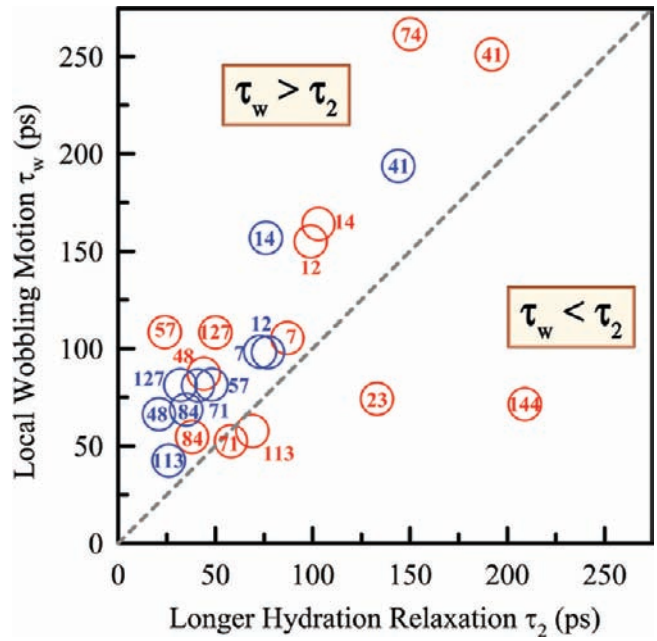

Figure 14. Comparison of the dynamics of tryptophan wobbling motion τ_ω, and longtime water-network relaxation τ_2. The mutants are labeled by circles with site numbers. Native state is in red, and molten globule is in blue. For most positions studied in apoMb, the hydration relaxation is faster than the wobbling motion, and only a few are special cases (see text).

The Hydration Speed and Water-Network Collectivity. To evaluate how fast the water networks relax in the hydration layer, only examination of relaxation times (τ_2 and τ_1) or energy shifts (ΔE_1 and ΔE_2) is not complete, and we need to define a rate of energy relaxation in cm^{-1}/ps. We define such an energy-drop rate as a hydration (solvation) speed (S) regardless of specific time and energy. Different mutants can have the similar hydration speed even though they have different relaxation times and energy shifts. Figure 10 shows S_1 and S_2 of all 29 proteins (16 mutants) and Figure 11 gives their relationship with the

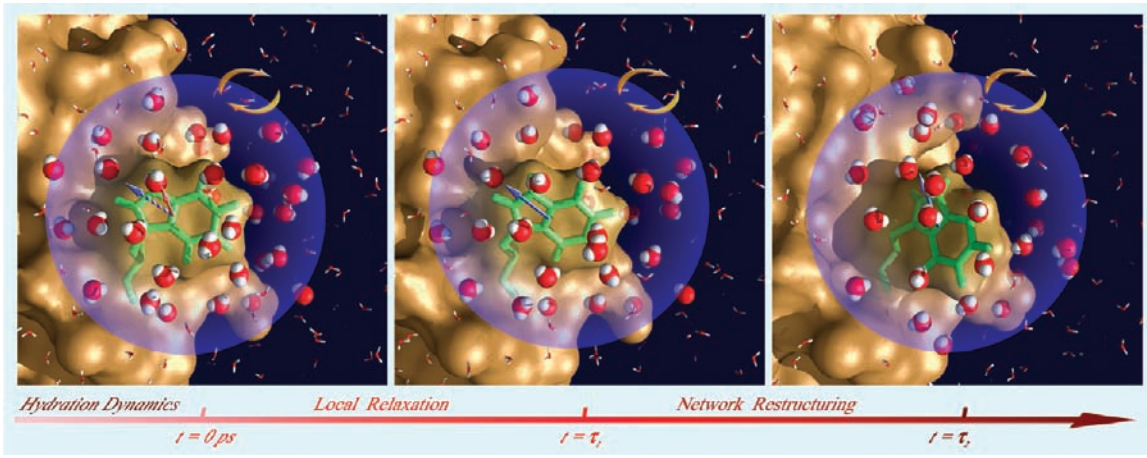

Figure 15. Snapshots of water motions in the hydration layer with one typical MD trajectory. Shown here is the A144W site with two water layers in the hydration shell. Only some water molecules in the shell within 7 Å from the indole ring are shown for clarity. The twin arrows show constant dynamical exchange of hydrating water molecules with bulk water. At time zero, the ground-state dipole moment of the indole upon photoexcitation is suddenly increased and reoriented (*left*). The neighboring hydrating water molecules rapidly rotate and translate at the local position in a few picoseconds (*middle*). The subsequent relaxation process is lateral water-network rearrangements coupled with local protein motions over tens of picoseconds (*right*), which gives rise to the slow component of the Stokes shift. During this process, some of the initial water molecules in the layer could be replaced by outside bulk water.

emission peaks of mutant proteins. Overall, both S_1 and S_2 are widely distributed and significantly heterogeneous. However, they clearly are larger in MG state than in N state, indicating that both the H-bond water networks (mainly S_1) and local protein structures (mainly S_2) become looser and more flexible.

Since the energy shifts (ΔE_1) become larger and the water motions (τ_1) get faster when the probe moves to the protein surface, the S_1 generally increases with λ_{max} shifted to the longer wavelengths (Figure 11A). Specifically, we categorize the S_1 values into five regions: (i) For four deeply buried probes of W14 (N and MG), H12W (N), A15W (N) and W7 (N), the S_1 is the smallest and ranges from 22 to 54 cm^{-1}/ps. Two partially buried mutants with the heavy (dense-)charged surroundings and higher-order structures, G23W (N) and A127W (N), also fall into this region; (ii) for partially exposed mutants of W7 (MG), A71W (N), H12W (MG), A74W (N), A71W (MG), H113W (N), the S_1 ranges from 86 to 132 cm^{-1}/ps. In addition, the solvent-exposed mutant of E41W (N) with the dense-charged surroundings has a similar hydration speed (106 cm^{-1}/ps); (iii) for mutants just located at the protein surface with certain higher-order structures, A22W (N), E41W (MG), H13W (MG) and T95W (N), S_1 has similar values between 198 and 258 cm^{-1}/ps. The partially buried mutant A127W (MG) close to the loop region at the end terminus and the fully exposed mutant A144W with the dense-charged surroundings are also in this region; (iv) for surface-exposed mutants of A84W (N and MG), A57W (N and MG), A22W (MG) in or near the loop regions, the S_1 ranges from 334 to 509 cm^{-1}/ps. The fully exposed mutant A144W (MG) with the dense-charged surroundings in the loop region also gives a similar hydration speed; and finally (v) for the mutants located at the protein surface in the loose loop regions, H48W (N and MG) and T95W (MG), the S_1 has the largest values from 667 to 831 cm^{-1}/ps. The classification of these regions is important and quantifies the hydration speed corresponding to local H-bond water-network rigidity, especially when the probe is located at the protein surface. Thus, the mutants with different environments could have similar hydration speed and H-bond water-network flexibility. Clearly, the solvation ability of H-bond water networks reflects hydration water-network's collectivity, which is related to its electrostatic interactions with the protein, i.e., local chemical identity of charged or hydrophobic residues and structural integrity of higher order and topological roughness.

The results for the hydration (solvation) speed of S_2 are interesting, and all S_2 values are much smaller than those of S_1 but have a linear relationship with their τ_2^{-1} with a slope of ~650 cm^{-1} (see inset in Figure 10B), resulting from the nearly constant ΔE_2 when the probe is located at the protein surface. Thus, the S_2 is directly related to τ_2, a key time scale of coupled water−protein fluctuations, having *no* direct relationship with the emission peaks (Figure 11B). All values of S_2 can be easily classified into three regimes: (i) For the mutants of E41W (N and MG), A144W (N), G23W (N), A74W (N) with dense-charged surroundings and the mutants with buried tryptophan, W14, H12W, A15W and H12W in both N and MG states, they have all similar S_2 values from 3 to 6.7 cm^{-1}/ps; (ii) for the mutants from H133W (N) to A84W (MG) in Figure 10B, the S_2 is directly related to the local structural flexibility and tertiary interactions, ranging from 8.7 to 18 cm^{-1}/ps. Many mutants nearly have the similar hydration speed; and finally (iii) in the loose loop regions, the mutants of T95W (N and MG), A57W (N) and H48 (MG) have the largest S_2 values from 25.8 to 32.2 cm^{-1}/ps. In addition, the H113W (MG) also falls in this class with a similar value of 24.4 cm^{-1}/ps (Figures 10B and 11B), and we believe that in the MG state, the H113 backbone becomes a loop or has a loop character. Similarly, the classification of S_2 is important because the S_2 directly evaluates the coupled water−protein fluctuations. Such quantification is useful and directly shows how fast the coupling dynamics of water networks with local proteins. Even for different mutants with various local structures and chemical identities, the resulting hydration (solvation) speed can be the similar as shown in Figures 10B and 11B. Clearly, the chemical properties such as dense-charged residues are critical to water−protein coupling motions and the hydration networks have the smallest solvation speeds and thus the largest collectivity due to strong electrostatic interactions.

The Local Protein Flexibility and Global Plasticity. The longer hydration dynamics of τ_2 and related hydration speed S_2 reflect the water-network restructuring in the interfacial layer

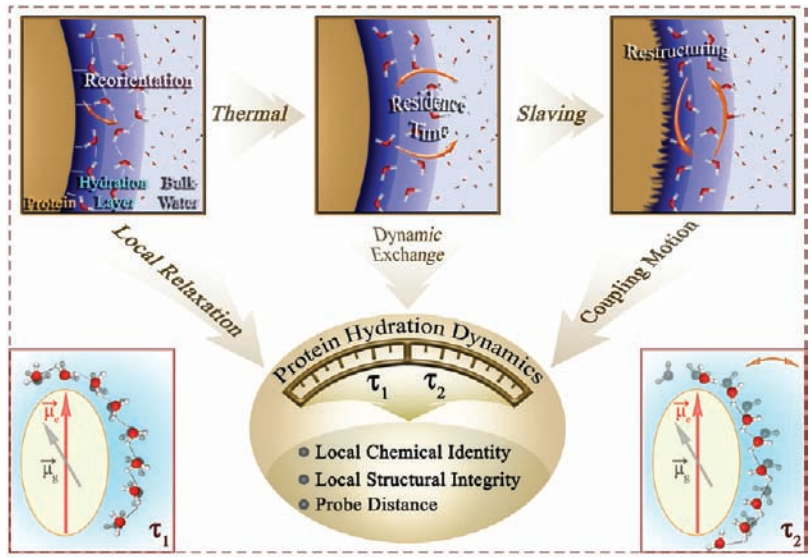

Figure 16. Unified molecular mechanism of protein hydration dynamics and coupled water−protein fluctuations. The initial ultrafast dynamics in a few picoseconds (τ_1) represents local collective water-network relaxation. On the longer time (τ_2), the water networks undergo structural rearrangements in the layer, strongly coupled with both local protein fluctuations and bulk-water dynamic exchange. The bottom two panels show such dynamic processes. The two types of water-network relaxations are strongly correlated with local protein chemical identities and structural rigidity.

from the initial nonequilibrium state to a final equilibrated configuration and such water-network rearrangements are facilitated by the coupling motions of hydrating water with local protein. Thus, local protein fluctuations must have certain relationship with the longer hydration dynamics. We examined all mutant rotational dynamics by measuring anisotropy decays. Figure 8A shows the restricted rotational motions of the probe tryptophan side chain in both N and MG states with a semi-angle from 12° to 26° and mostly in 16−18°. However, their wobbling dynamics (τ_w) occur in a wide time range from 52 ps (A71W) to 262 ps (A74W), a reflection of their different local structural constraints and electrostatic interactions, i.e., local protein compactness and rigidity. These dynamics are also correlated well with local protein properties. In N state, the hydrophobic site of A71W has the shortest wobbling time, consistent with less electrostatic interactions. For the two mutants of H113W and G23W with the smallest rotating space, they take less rotational relaxation time (58−74 ps). For the mutants in the loop regions or close to the end termini of helices (A84W, A144W, H48W, W7, A127W and A57W), the wobbling dynamics are well correlated with their structural rigidity (55−81 ps). For the two buried sites of H12W and W14 inside the hydrophobic core, the rotational dynamics take a longer time of ∼160 ps. Finally, for the two dense-charged sites with higher-order structures (E41W and A74W), the rotational relaxations are the slowest even in about 260 ps.

In MG state, all of the wobbling angles except A57W and A144W become larger (Figure 8A), and the structure becomes looser. For A57W mutant, as observed in the hydration dynamics with the slower relaxation (Figure 6), the D-helix extends longer, and the local structure becomes more rigid, resulting in a smaller wobbling angle. The A144W mutant becomes a loose loop at the C terminal, and both the probe tryptophan and the loop proceed to the wobbling motions like the mutant T95W. Both motions are coupled, and the angle in Figure 8A for MG state could be underestimated. Similarly, all wobbling dynamics of mutants except A71W and A84W become faster, indicating that the MG structure becomes soft with larger global plasticity. For A71W and A84W, both emission peaks shift to the blue side by 2−3 nm and the probes move inside the protein with more electrostatic and structural interactions, resulting in the longer relaxation times.

To reflect the local flexibility, the average angular speed should be a better variable. As shown in Figure 8C, in N state the dense-charged sites (A74W and E41W) have the slowest rotational speed of less than 0.1 deg/ps. Second, the angular speeds are well correlated with the probe locations from buried, to partially buried and to fully exposed in 0.15−0.31 deg/ps. Finally, the probe (A71W) in the hydrophobic patch has the fastest rotational speed in 0.32 deg/ps. In MG state, nearly all probes rotate faster than in N state, resulting from a looser structure and reflecting larger global plasticity in MG state. Similarly, A84W and A71W mutants have the smaller angular speeds due to the probe more buried inside the protein in MG state. Again, for H113W, the angular speed in MG state is largest in 0.44 deg/ps, similar to the loop probe of H48W and A144W, further indicating the loop nature of H113W in MG state.

To further examine the plasticity of the protein, we show in Figure 12 the angular speeds relative to the tryptophan emission peaks, i.e., the relative probe locations to the protein surface. For most mutants, the angular speeds of the probe are well correlated with the emission peaks. The more exposed the probe, the more flexible the local structure shows. This observation is striking and indicates gradual changes of flexibility from the inner protein to the outerside surface, reflecting the inside rigid compactness and the surface softness. The mutants of A74W (N) and E41W (N and MG) have relatively smaller angular speeds due to the dense-charged environments. The H113W (MG) and A71W (N) have relatively larger angular speeds due to the loose loop and hydrophobic surrounding, respectively. The definition of the angular speed here may provide a useful way to evaluate local flexibility and global plasticity within a protein or between different proteins.

The Intimate Coupling of Water−Protein Fluctuations. Figure 13 shows the final mapping of the hydration dynamics, water−protein fluctuations and local protein motions around the protein surfaces in N and MG states using the obtained local hydration speeds, S_1 and S_2, and tryptophan's angular speeds, ω. Globally, all water motions and protein fluctuations become

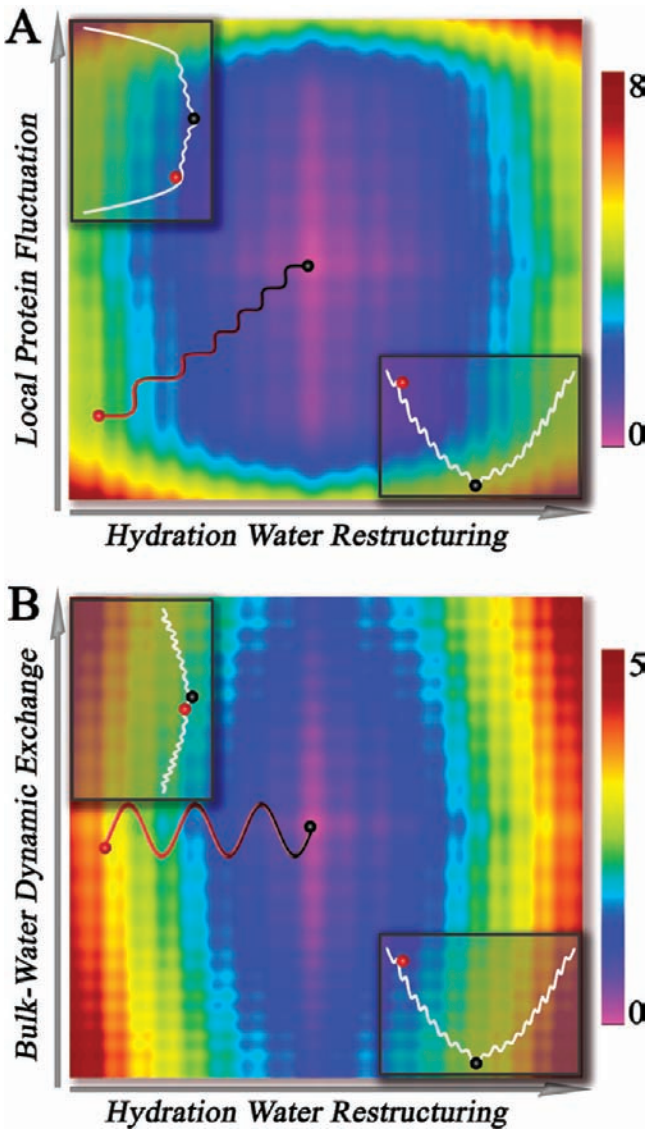

Figure 17. Schematic contour representation of the energy landscape for the longtime water-network dynamics along three coordinates: water-network arrangement in the hydration layer, coupled local protein fluctuation, and bulk-water dynamical exchange. (A) The nonequilibrium hydrating water molecules evolve into a new equilibrated configuration, and along the pathway such water-network rearrangements couple with local protein motions. The protein fluctuates among many substates coupled with the water-network relaxation. (B) The water networks evolve along the minimum energy path and meanwhile have a dynamic exchange with bulk water on the similar time scale. The bulk water fluctuates around its equilibrium state.

faster in MG state than in N state, reflecting the coupling between hydration water and the protein and the loss of the H-bond water-network collectivity and protein structural integrity. Individually, the mutants show significant heterogeneity, and their dynamics strongly depend on local specificity. Hydration water motions are strongly coupled with local protein properties, especially local chemical identities and higher-order structures. The hydrophobic core (A-G-H helices) is more rigid than the heme-binding site (B−H helices), reflecting structural stability and functional flexibility.

The observed, second long hydration dynamics is a long collective relaxation process of H-bond water-network rearrangements from the initial nonequilibrium to a final new equilibrium. These water cooperative motions are strongly coupled with protein fluctuations, and thus, the time scales (τ_2) should have certain relationships with the local side-chain motions (τ_w). Figure 14 shows such correlation, and overall, except for the mutants of A144W, G23W and H113W, and A71W, the probe's wobbling times are longer than the local hydration water relaxations, clearly indicating that local hydration network relaxation is faster than local protein side-chain motion and such two dynamics of hydrating water and protein side chains are not equal. Given by the small wobbling rotational angles of the probes (Figure 8A), the water networks completely finish cooperative restructuring, while the probe side chains only proceed to a small wobbling motion in a very constrained cone angle. This observation is significant, indicating that local protein fluctuations, facilitated initially by fast water motions in the layer, further assist water-network rearrangements, and such coupled motions (back and forth) collectively search for the minimum basin on the energy landscape.

Among four exceptions, the probe tryptophan of A144W mutant has a dense-charged surrounding, and the water networks in the layer have much stronger collectivity, resulting in a long relaxation time in 209 ps. However, the probe is fully exposed to water and has less intraprotein interactions with nearby side chains. The wobbling motion becomes relatively easier in 71 ps. Basically, the probes take three times as many of the wobbling rotations to accommodate the complete water-network cooperative relaxation. Similarly, for G23W, the dense-charged environment results in a long relaxation time of local water networks, but the probe is highly restricted due to the tertiary intraprotein interactions with a very small wobbling angle (Figure 8A). For H113W, the probe has the smallest wobbling rotational angle (11.7°), and for A71W, the probe is in a hydrophobic environment. Both mutants have the similar time scales for hydration water-network relaxation and local probe wobbling motion, indicating that one complete rotational motion of the probe is enough to facilitate the entire water-network rearrangements. It should be pointed out that all these local probe rotational motions are very small in a semi-cone angle of 10−15°. Such constrained local rotations, coupled with hydration water, assist collective water-network lateral restructuring.

Recent MD simulations have provided deep insights into the coupled water−protein fluctuations[79,83,84,87−90] although significant quantitative discrepancies still exist, especially about the total relaxation energy (ΔE), initial ultrafast water motions, and the origin of second slower solvation dynamics.[79,83,84] Figure 15 shows three snapshots from a 500-ps nonequilibrium trajectory of MD simulations for A144W mutant. Upon sudden change of the dipole moments of the probe, the nearby hydration water proceeds to local reorientational and small translational motions (τ_1) with a significant energy drop (ΔE_1). Currently, the simulated time and energy are much shorter and larger than the experimental results, respectively. Subsequently, the water networks make lateral structural arrangements, and meanwhile the hydration water dynamically exchanges with bulk water in tens of picoseconds (residence time). These cooperative, convoluted motions result in the significant replacement of original

(87) Pizzitutti, F.; Marchi, M.; Sterpone, F.; Rossky, P. J. *J. Phys. Chem. B* **2007**, *111*, 7584–7590. Giovambattista, N.; Lopez, C. F.; Rossky, P. J.; Debenedetti, P. G. *Proc. Natl. Acad. Sci. U.S.A.* **2008**, *105*, 2274–2279. Lopez, C. F.; Darst, R. K.; Rossky, P. J. *J. Phys. Chem. B* **2008**, *112*, 5961–5967.
(88) Hassanali, A. A.; Li, T.; Zhong, D.; Singer, S. J. *J. Phys. Chem. B* **2006**, *110*, 10497–10508.
(89) Bizzarri, A. R.; Cannistraro, S. *J. Phys. Chem. B* **2002**, *106*, 6617–6633.
(90) Gilmore, J.; McKenzie, R. H. *J. Phys. Chem. A* **2008**, *112*, 2162–2176.

water molecules in the layer with bulk water and the hydrating water molecules finally reaching the new equilibrated configuration. By either freezing protein fluctuations or hydration water motions, the longtime lateral water-network restructuring will disappear, directly supporting the coupled longtime fluctuations between interfacial water and the protein. This intimate coupling is a direct reflection of local protein fluctuations, a key determinant for biological function.

Conclusion

We report here our direct mapping of global surface hydration dynamics and water−protein coupling fluctuations around an α-helical globular protein of apomyoglobin in both native and molten globule states. With site-directed mutagenesis, 16 single-tryptophan mutants, one at a time, were designed to cover different local environments, structural and chemical, and to scan the entire protein surface. With the femtosecond resolution, we systematically examined water motions near the termini, loose loops, rigid helices, hydrophobic patches and different dense-charged amino acid clusters in the hydration layer. We observed robust biphasic hydrating water-network motions on two distinct time scales. One is in a few picoseconds, and the other ranges from tens to hundreds of picoseconds. Both water-network dynamics show significant heterogeneity from site to site and strongly correlate with the local protein properties. A series of correlations of both energy relaxation and dynamical motion with the local chemical identity and structural integrity were observed that helped to elucidate the origin of different hydrating water motions in the layer and to reveal the nature of water−protein coupling fluctuations. To quantify the hydrogen-bond water-network rigidity and local protein flexibility, we also defined a hydration (solvation) speed for water relaxation and an angular speed for side-chain wobbling motion from anisotropy dynamics. From native to molten globule states, all hydration dynamics become faster, the water networks in the shell loosen up, and the protein becomes more flexible. All these results are summarized in Figures 16 and 17 and provide molecular insights into protein hydration dynamics and coupled water−protein fluctuations at the most fundamental level.

The striking observation of the energy relaxation (Stokes shifts) in two distinct distributions relative to the probe's location unambiguously shows the dominant contributions from water molecules in the hydration layer. The first contribution is from all water molecules in the detection range in the hydration shell, and the second one is only from the inner interfacial rigid hydrating water in the layer. This observation also explains the fluorescence emission patterns of tryptophan in the textbook,[80] i.e. the emission peak of surface tryptophan is around 340 nm or longer, regardless of its neighboring protein environments, hydrophobic or hydrophilic. The different local properties of this globular protein only result in a fluctuation of second energy relaxation less than 12%; the hydration water relaxation in the layer is dominant, and the protein contribution is minor.

The corresponding two time scales are very informative and show a series of correlations with protein properties, chemical and structural. The first time scale consists of a few picoseconds, much slower than that observed in bulk water by 1 order of magnitude. Such initial water dynamics are local collective H-bond water-network relaxation, and these water molecules are highly structured. The rigidity of the water networks is strongly correlated with local chemical identities, especially charged amino acids due to strong electrostatic interactions (Figures 6A, 9A and 11A). This local initial collective relaxation reflects the water-network flexibility, which is determined by water−protein interactions and water-network collectivity. The time scale in few picoseconds reveals the collective nature of H-bond network dynamics in the hydration layer. The initial ultrafast hindered motions observed in bulk water are highly suppressed and dramatically slowed down due to highly structured water networks in the hydration layer. On the basis of the observed initial water dynamics, we found that the dynamic hydration layer extends to more than 10 Å.

The second time scale ranges from tens to hundreds of picoseconds and truly reflects the coupled water−protein fluctuations at the interface. Significantly, the energy relaxation is dominantly from the interfacial water molecules in the inner layer, and thus the dynamics are coupled with local protein motions on this time scale. For a given rigid protein structure as shown in recent MD simulations,[79] such coupled water−protein motions in the layer cease, and the lateral rearrangements of water networks are eliminated. However, the longitudinal dynamical exchange with bulk water still occurs, typically on a similar time scale of tens of picoseconds (residence time). For a soft protein surface, local protein fluctuations are facilitated by such longitudinal water dynamics, and to make rearrangements laterally water networks in the inner layer must couple with protein fluctuations and bulk-water dynamical exchange (Figures 16 and 17). Such coupled motions between water networks and the protein, back and forth, from the initial nonequilibrium to a final equilibrated configuration are illustrated in Figure 17A. Although the local protein fluctuations are highly constrained in very small space (Figure 8), the actual coupled water−protein motions depend on local protein chemical identity, topological roughness, higher-ordered structure and tertiary intraprotein interaction. The strong correlations of the coupled motions with chemical property and structural rigidity of the local protein were observed with wide heterogeneity on the picosecond time scales. Such coupled longtime water relaxations reflect the local cooperativity and lateral mobility of water networks in the layer and reveal the nature of local water−protein fluctuations, which are determinants for biological functions such as in searching for a local minimum in protein folding, maintaining structural intactness and flexibility, lubricating protein recognition and binding, and mediating catalytic enzyme reactions at active sites.[3,12]

Acknowledgment. We thank Profs. Ahmed Zewail (Caltech) and Sherwin Singer (Ohio State Univ.) for the helpful discussion. We also thank Prof. Stephen Sligar (Univ. of Illinois at Urbana−Champaign) for providing us the myoglobin plasmid (pMb122), Prof. Dehua Pei (Ohio State Univ.) for providing us the use of his biochemical equipment for initial preparing of protein samples, Drs. Wenyun Lu, Weihong Qiu and Mr. Oseoghaghare Okobiah for the partial help with the experiments, and Tanping Li for calculation and preparation of Figure 15. The work was supported in part by the National Science Foundation, the Packard Foundation fellowship, the Sloan fellowship, the Camille Dreyfus Teacher-Scholar award and the endowed Robert Smith Professorship.

Supporting Information Available: Table 1S of all fitting parameters for mutant A71W transients in two states, Table 2S of all fitting parameters for correlation functions of all mutants, and Table 3S of all fitting parameters of their rotational anisotropy dynamics. This material is available free of charge via the Internet at http://pubs.acs.org.

JA902918P